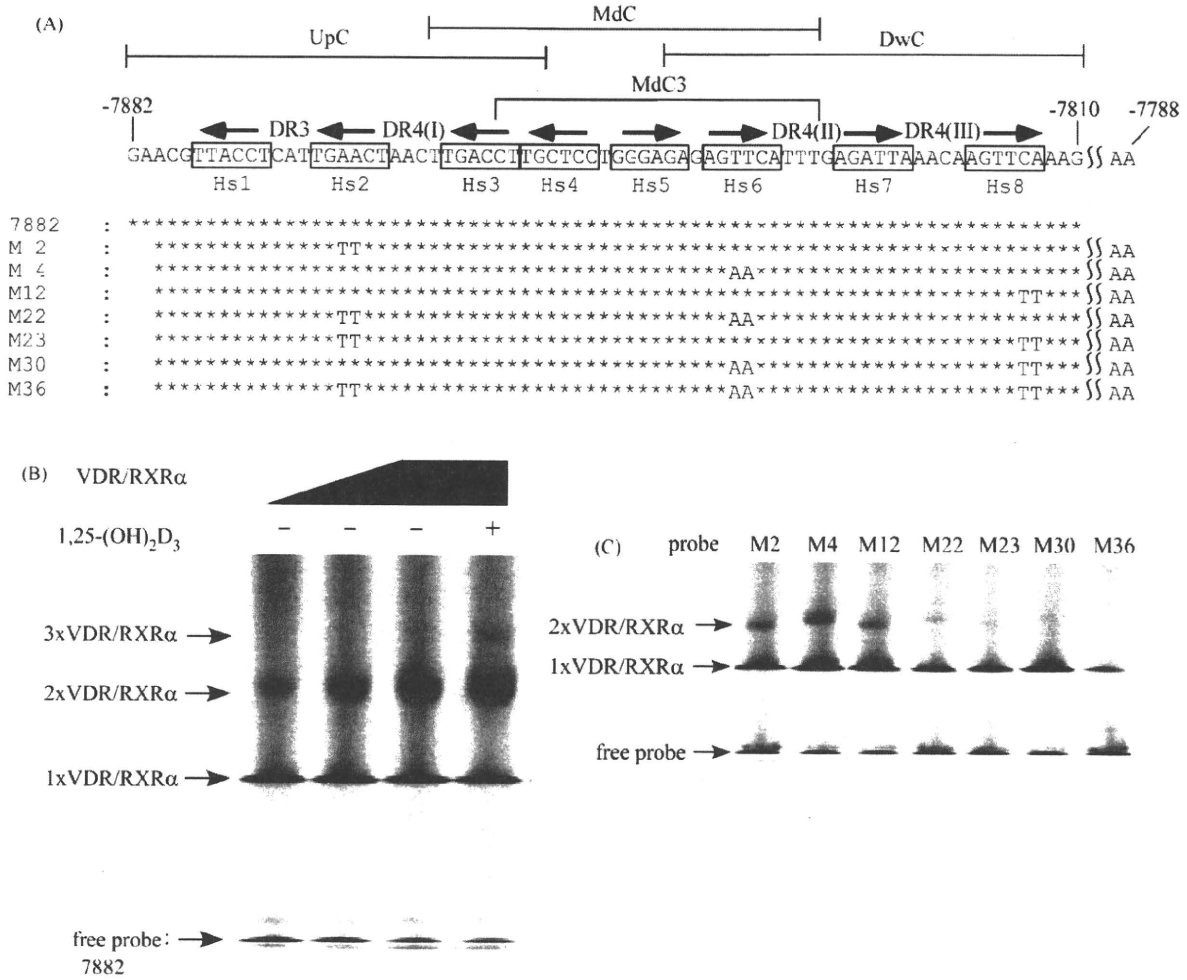

Fig. 3 – VDR/RXRα can bind to three VDR-binding sites at the same time. (A) The oligonucleotide sequences used for EMSA. Putative half-sites are boxed and arrows indicate the direction of the half-site. Numbers are in reference to the transcriptional start site at +1. Only nucleotides that differ from the wild-type are shown as letters; asterisks represent unchanged nucleotides. (B) EMSA was performed using a FITC-labeled 7882 probe. The probe was incubated with the increasing amount of in vitro translated VDR and RXRα as described in Section 2. The complexes were resolved by electrophoresis on a 2.8% Long Ranger gel. (C) EMSA was performed using several FITC-labeled probes, shown in (A). The probes were incubated with 1,25-$(OH)_2D_3$ and in vitro translated VDR and RXRα as described in Section 2. The complexes were resolved by electrophoresis on a 2.8% Long Ranger gel.

When all three half-sites were mutated (M36), the upper and middle bands disappeared and the lower band significantly decreased. These data indicate that one molecule of VDR/RXRα binds to each element including Hs2, Hs6, or Hs8. Consequently, three molecules of VDR/RXRα bind simultaneously to this region.

3.4. *VDR-binding sites located between −7880 and −7810 bp mediate the transactivation of MDR1 by 1,25-$(OH)_2D_3$*

In the experiments described above, we identified several VDR-binding sites. To test if these sites are functional, the same mutations introduced into the probes and competitors in the EMSA were introduced into the pMD*824Δ90L construct for use in the luciferase assay. The names of these mutants correspond to those used in the EMSA. The mutated regions of the constructs used for the luciferase assays are summarized in Fig. 4A. As shown in Fig. 4B, the mutation in Hs4 (M31) or Hs5 (M33), although slightly increased induction, had no apparent effect on inducibility, indicating that these half-sites play no significant role in induction by 1,25-$(OH)_2D_3$. The other mutations introduced into individual half-sites (M1, M2, M3, M4, M7, and M12) lead to decreased inducibility. The mutations introduced simultaneously into the two half-sites in two of the three segments resulted in a further decrease in induction by 1,25-$(OH)_2D_3$ (M28, M26, M29, M22, M27, M23, M30 in Fig. 4B). M22 and M29 (mutations in Hs2 and Hs6, and Hs3

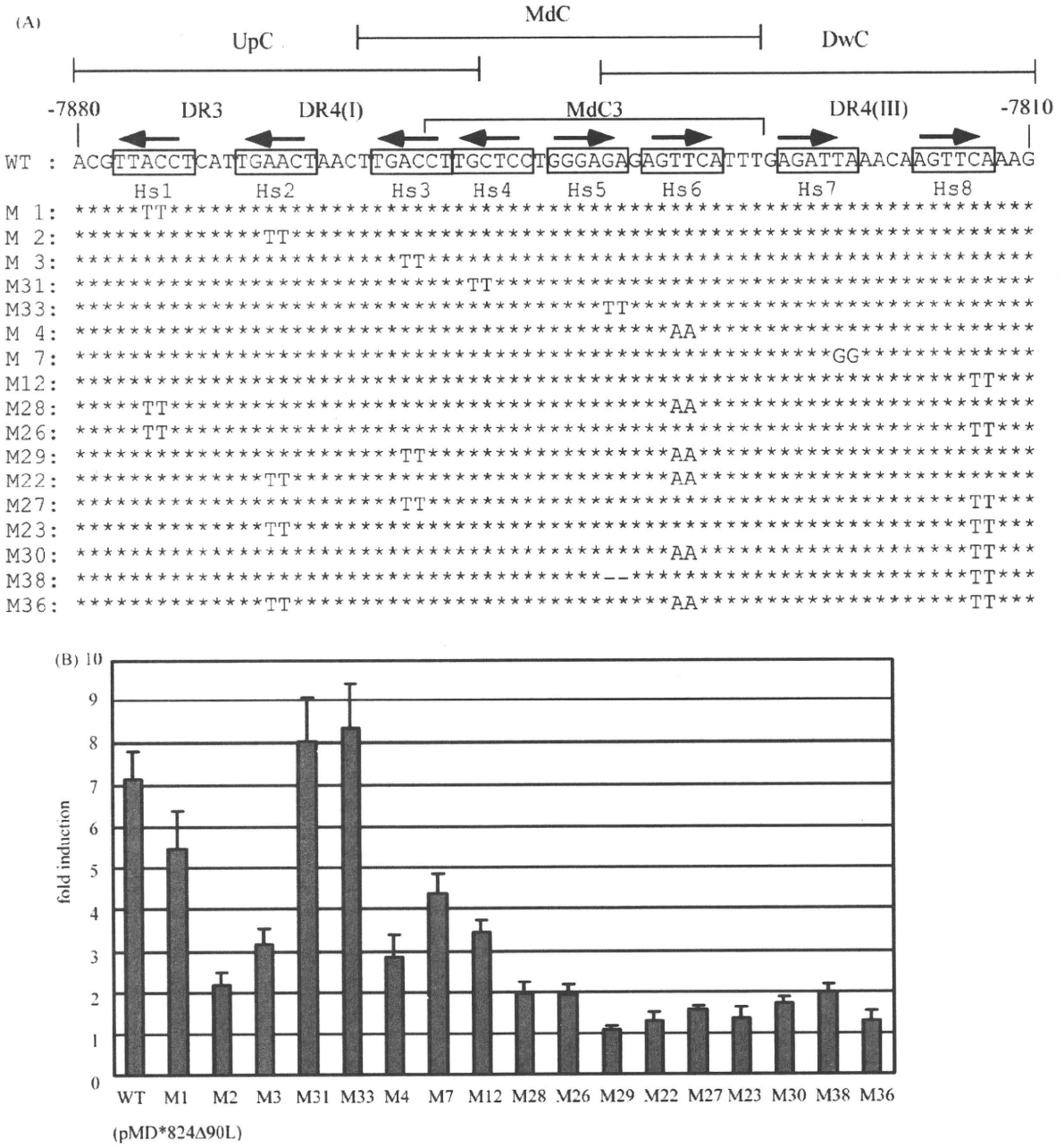

Fig. 4 – VDR-binding sites between −7880 and −7810 bp mediate the transcriptional activity of *MDR1* by 1,25-$(OH)_2D_3$. (A) Several mutations were introduced into the pMD*824Δ90L plasmid (designated WT). Putative half-sites are boxed and arrows indicate the direction of the half-site. Asterisks denote bases identical to the wild-type sequence and letters indicate the bases altered in the mutated sequences. The underbar indicates deletion of a nucleotide. Numbers are in reference to the transcriptional start site at +1. (B) The luciferase activity was analyzed as described in Section 2. The fold induction was calculated as the radio of luciferase activity in 1,25-$(OH)_2D_3$-treated cells to that of DMSO-treated cells. Each value represents the mean ± S.D. of four independent experiments.

and Hs6, respectively) almost abolished inducibility. The inducibility of M38, which has the deletion of one of the three repeated AGs located between Hs5 and Hs6 in M12 (Fig. 4A), decreased more than that of M12 (Fig. 4B). The inducibility of M36, which has mutations in all three segments, was also almost abolished. These results indicate that every half-site in the VDR-binding sites, except Hs4 and 5, is a functional VDRE and makes its own contribution to induction by 1,25-$(OH)_2D_3$. Furthermore, each VDRE additively contributes to the 1,25-$(OH)_2D_3$ response.

4. Discussion

Several studies have shown that 1,25-$(OH)_2D_3$ induces the expression of *MDR1* [7,22]. However, it remains unclear how 1,25-$(OH)_2D_3$ regulates *MDR1* expression. In this study, we demonstrated that the induction of *MDR1* by 1,25-$(OH)_2D_3$ is mediated by VDR/RXRα binding to the region located between −7.9 and −7.8 kbp upstream from the transcriptional start site of the human *MDR1* gene (Fig. 5).

As shown in Fig. 1B, the region located between −7880 and −7817 bp is essential for VDR-mediated induction. This result is the same as that obtained for TR-mediated induction [19]. Furthermore, this region overlaps with the previously identified PXR-, CAR-responsive region [3,4]. The eight putative half-sites (Hs1–Hs8) of VDREs were found in the region located between −7880 and −7810 bp (Fig. 2A). DR3, DR4(I), DR4(II), and DR4(III), which were previously designated by Geick et al., are composed of Hs1 and Hs2, Hs2 and Hs3, Hs6 and Hs7, and Hs7 and Hs8, respectively. Geick et al. reported that PXR/RXRα bound to these three DR4, with the highest affinity to DR4(III), and DR4(I) is an important element for PXR-mediated induction [3]. Burk et al. reported that CAR bound to DR4(I) and DR4(III) as a heterodimer with RXRα, and to the 5′-half-site of DR4(II) (designated as Hs6 in this study) as a monomer [4]. As for transcriptional activity, DR4(I) and the 5′-half-site of DR4(II) were reported to be important elements for CAR-mediated induction. Recently, we reported that TR/RXRα bound to UpC [including DR3 and DR4(I)] and DwC [including DR4(II) and DR4(III)] segments [19], whereas TR/RXRα did not bind to MdC located between UpC and DwC (M. Saeki, K. Kurose, unpublished data). Furthermore, two molecules of TR/RXRα bind simultaneously to the region, and several DRs contribute to the binding affinity in the order: DR4(I) > DR4(II) > DR3 ≈ DR4(III). As for the transcriptional activity, every direct repeat contributes to TR-mediated induction [19]. In the present study, we showed that VDR/RXRα bound to UpC (including Hs1–3), MdC (including Hs3–6), and DwC (including Hs6–8) (Fig. 2B). To date, no nuclear receptors other than VDR has been reported to bind to MdC by forming heterodimers with RXRα. Although Hs6, which is located at the overlapping region between MdC and DwC, significantly contributes to induction by CAR [4], the binding of CAR/RXRα to MdC and contribution of MdC to induction by CAR remains to be elucidated. As shown in Fig. 2B, the relative binding affinity of the VDR-binding elements is DR4(I) > DR3 > MdC3 > DR4(III) > DR4(II). Consequently, the relative binding ability of VDR to these elements located in this region is clearly different from that of PXR, CAR, and TR, though the VDR-responsive region overlaps with the PXR-, CAR-, and TR-responsive regions [3,4,19]. The overlapping of nuclear receptor-responsive regions was also observed on the other genes such as CYP3A4 [23], in which PXR/RXRα and CAR/RXRα exhibited similar binding affinity toward proximal ER6 element [24]. On the nuclear receptor-responsive region of *MDR1* gene, PXR/RXRα and CAR/RXRα bound to DR4(I) with similar affinity, although PXR/RXRα bound to DR4(III) with the higher affinity than CAR/RXRα [4]. Although, relative binding affinities among TR/RXRα, VDR/RXRα, PXR/RXRα, and CAR/RXRα to these binding elements have not been examined, it is conceivable that cooperative effects of the nuclear receptors with different binding affinities, tissue distributions and ligand concentrations affect the expression of *MDR1*.

Three shifted bands were observed when a longer probe including all the half-sites of the VDR-binding elements was used for EMSA (Fig. 3A). The upper band (3× VDR/RXRα) was found to be enhanced by 1,25-$(OH)_2D_3$. This has also been observed in VDREs located in several genes such as human CYP24 [25-27] and is due to the stabilization of DNA–VDR/RXRα formation by 1,25-$(OH)_2D_3$ [26,28,29]. The relative binding affinity of the VDR-binding elements estimated from Fig. 2B is DR4(I) > DR3 > MdC3 > DR4(III) > DR4(II). The affinity was examined further by using each discrete oligonucleotide as a competitor and a probe. Fig. 3 indicates that three molecules of VDR/RXRα bind simultaneously to the region, and one molecule of VDR/RXRα binds to each element including Hs2, Hs6, or Hs8. It is obvious that the element including Hs8 is DR4(III); consequently, the element including Hs6 is in MdC3, but it could not be specified further. Although both DR3 and

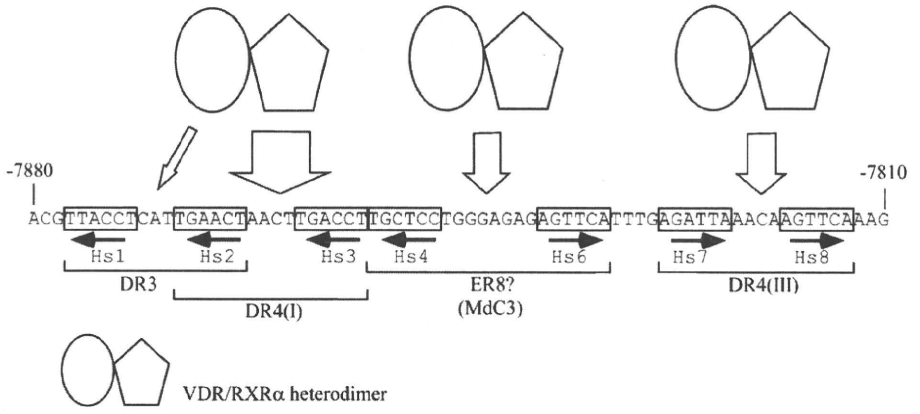

Fig. 5 – Three molecules of VDR/RXRα bind to VDREs located −7.9 to −7.8 kb upstream of the *MDR1* gene with different affinities. The nucleotide positions are shown relative to the transcription start site of *MDR1*. The half-sites of the VDREs are boxed with arrows. VDR/RXRα binds to DR3 or DR4(I), ER8, and/or DR4(III) with different affinity, which is denoted by the thickness of the arrow.

DR4(I) include Hs2 and each alone shows high affinity to VDR/RXRα, two molecules of VDR/RXRα are not able to simultaneously bind to DR4(I) and DR3 because they overlap with Hs2 (Fig. 2A). Therefore, judging from the binding affinity and decreased inducibility from the reporter gene assay (Fig. 4B), three molecules of VDR/RXRα would mainly bind to DR4(I), MdC3, and DR4(III) simultaneously. The middle band intensity of the M4 probe (MdC3 mutation) was stronger than that of the M2 and M12 probes (DR4(I) and DR4(III) mutations, respectively) (Fig. 3C). The difference in the middle band intensity between the M4 and M12 probes in Fig. 3C suggests that the two molecules of VDR/RXRα simultaneously bind to DR4(I) and DR4(III) more strongly than to DR4(I) and MdC3, though the relative binding affinity of VDR/RXRα to MdC3 was higher than to DR4(III), as shown in Fig. 2B. The proximity of DR4(I) and MdC3 might slightly restrict the binding of the two molecules of VDR/RXRα to those sites simultaneously.

We confirmed whether the VDR-binding sites contribute to induction using constructs with mutations in several half-sites (Fig. 4). DR4(I) and DR4(III) contribute to induction by 1,25-$(OH)_2D_3$, and so are functional VDREs. MdC3 includes Hs4, Hs5, and Hs6. Although the mutation in Hs6 (M4) resulted in reduced inducibility, both the mutation in Hs4 (M31) and that in Hs5 (M33) had little effect on induction (Fig. 4B). Precisely which half-site is paired with Hs6 is unclear, but Hs6 contributes to induction by 1,25-$(OH)_2D_3$. However, when one AG deletion of the three repeated AGs, which are located just upstream of Hs6 (Fig. 4A), was introduced into M12, the inducibility of the resulting mutant construct M38 decreased more than that of M12 (Fig. 4B). This indicates that the deletion results in reduced inducibility, suggesting that the half-site paired with Hs6 is located upstream of Hs6, and that the change in the spacer length between Hs6 and its upstream partner leads to the reduced inducibility. Hs4 is located upstream of Hs6, and the mutation introduced in Hs4 reduced binding activity (Fig. 2C, Md3M31). Therefore, the partner of Hs6 might be Hs4, although the mutation of Hs4 alone did not reduced inducibility by 1,25-$(OH)_2D_3$ (Fig. 4B, M31). If Hs4 and Hs6 are partners, then they are an everted repeat by 8 nucleotides (ER8). The mutation in Hs1 (Fig. 4B, M1, M28, and M26), namely the mutation in DR3, caused somewhat decreased activity. Thus, DR3 can function as a VDRE, suggesting that DR3 serves as an auxiliary function of the neighboring DR4(I) element.

Double mutations in the different segments result in substantial reduction in induction by 1,25-$(OH)_2D_3$ (Fig. 4). Among them, the double mutations in DR4(I) and ER8 of MdC3 resulted in an almost complete loss of inducibility (M22 and M29 in Fig. 4B). In M22, only DR4(III) is a wild-type motif, and in M29, DR3 is a wild-type motif in addition to DR4(III). Therefore, DR4(III) alone or in combination with DR3 might be incapable of induction. However, DR4(III) works cooperatively in combination with DR4(I) and/or MdC3 (compare M2 with M23, M4 with M30, and WT with M12 in Fig. 4B). These results indicate that the additive binding of VDR/RXRα to several VDREs results in additional enhancement of *MDR1* induction by 1,25-$(OH)_2D_3$.

Previous reports showed that Caco-2 cells are clearly less sensitive to the inductive effect of 1,25-$(OH)_2D_3$ compared with LS180 cells [7,30]. The VDR mRNA level in Caco-2 cells is lower than that in LS180 cells (twofold higher band intensity in LS180 cells) [9]. Additionally, the ligand-binding assay showed that LS180 and Caco-2 have VDR levels of 118 and 63 fmol/mg protein, respectively [31]. In our preliminary luciferase reporter experiment using LS180 cells transfected by pMD*824Δ90L, which contains VDREs, we observed transcriptional induction by 1,25-$(OH)_2D_3$ even in the absence of VDR expression plasmid (data not shown). Thus, the difference in response to 1,25-$(OH)_2D_3$ between these cells may reflect the amount of VDR/RXRα, which binds to the VDREs in the *MDR1* gene. VDR is expressed abundantly in the human intestine (approximately 250 fmol/mg protein) [32,33]. Thus, it is possible that 1,25-$(OH)_2D_3$ is involved in intestinal *MDR1* expression under normal physical conditions. Recent reports demonstrated that CYP27B1, which has an important role in the synthesis of 1,25-$(OH)_2D_3$, is expressed in human intestine [34–36]. In addition, extrarenally produced 1,25-$(OH)_2D_3$ primarily serves as an autocrine/paracrine factor with cell-specific functions [37,38]. Therefore, 1,25-$(OH)_2D_3$ levels in the intestine might be relatively high, whereas serum 1,25-$(OH)_2D_3$ levels are usually controlled at approximately 100 pmol/L. *MDR1* expression levels are different between individuals [20], and these variations might affect the toxicity and efficacy of drugs. Intestinal vitamin D status, which might be affected by, for example, intestinal CYP27B1 and circulating 25-hydroxyvitamin D_3 levels, might partially contribute to differences between individuals in *MDR1* expression.

Recently, it has been shown that 1,25-$(OH)_2D_3$ is involved in the formation of tight junctions, which seal the paracellular space between adjacent cells to create a primary barrier, in intestinal epithelial cells [39]. Kutuzova et al. reported that 1,25-$(OH)_2D_3$ causes increases in the expression of several phase I and phase II enzymes such as CYP3As in rat intestine after injection of 1,25-$(OH)_2D_3$ into vitamin D-deficient rats [40]. These data indicate that 1,25-$(OH)_2D_3$ would play an important role in the intestinal epithelial barrier function against xenobiotics by regulating tight junctions and inducing several drug-metabolizing enzymes and *MDR1*.

The induction of P-gp by 1,25-$(OH)_2D_3$ could lead to an increase in the systemic efflux of co-administrated drugs that serve as P-gp substrates. For instance, Olaizola et al. reported that the uptake of [^{99m}Tc]-sestamibi by the parathyroid glands of uremic patients was suppressed by pulse administration of 1,25-$(OH)_2D_3$ [13]. [^{99m}Tc]-Sestamibi is a substrate of P-gp and is excreted by P-gp [11,12], suggesting that P-gp induction by 1,25-$(OH)_2D_3$ leads to increased efflux of [^{99m}Tc]-sestamibi [13]. Vitamin D derivatives are widely prescribed, therefore, consideration for drug–drug interaction mediated by induction of P-gp by vitamin D derivatives should probably be paid.

In summary, we have demonstrated that the induction of *MDR1* by 1,25-$(OH)_2D_3$ is mediated by VDR/RXRα binding to VDREs located between −7.9 and −7.8 kbp upstream of the human *MDR1* gene, and that three molecules of VDR/RXRα are able to simultaneously bind with different affinities. DR3, DR4(I), MdC3 (ER8) and DR4(III) are functional VDREs, and the contribution of each VDRE toward inducibility is different (Fig. 5). Furthermore, each VDRE additively contributes to the 1,25-$(OH)_2D_3$ response.

Acknowledgements

We thank Dr. Shuichi Koizumi (Yamanashi University) for providing the human RXRα cDNA. This work was supported in part by grants from the Ministry of Health, Labor and Welfare of Japan and the Japan Health Sciences Foundation (Research on Publicly Essential Drugs and Medical Devices).

REFERENCES

[1] Marchetti S, Mazzanti R, Beijnen JH, Schellens JH. Concise review: clinical relevance of drug drug and herb drug interactions mediated by the ABC transporter ABCB1 (MDR1, P-glycoprotein). Oncologist 2007;12:927–41.
[2] Wacher VJ, Wu CY, Benet LZ. Overlapping substrate specificities and tissue distribution of cytochrome P450 3A and P-glycoprotein: implications for drug delivery and activity in cancer chemotherapy. Mol Carcinog 1995;13: 129–34.
[3] Geick A, Eichelbaum M, Burk O. Nuclear receptor response elements mediate induction of intestinal MDR1 by rifampin. J Biol Chem 2001;276:14581–7.
[4] Burk O, Arnold KA, Geick A, Tegude H, Eichelbaum M. A role for constitutive androstane receptor in the regulation of human intestinal MDR1 expression. Biol Chem 2005;386:503–13.
[5] Bertilsson G, Heidrich J, Svensson K, Asman M, Jendeberg L, Sydow-Backman M, et al. Identification of a human nuclear receptor defines a new signaling pathway for CYP3A induction. Proc Natl Acad Sci USA 1998;95:12208–13.
[6] Moore LB, Parks DJ, Jones SA, Bledsoe RK, Consler TG, Stimmel JB, et al. Orphan nuclear receptors constitutive androstane receptor and pregnane X receptor share xenobiotic and steroid ligands. J Biol Chem 2000;275:15122–7.
[7] Aiba T, Susa M, Fukumori S, Hashimoto Y. The effects of culture conditions on CYP3A4 and MDR1 mRNA induction by 1alpha,25-dihydroxyvitamin D(3) in human intestinal cell lines, Caco-2 and LS180. Drug Metab Pharmacokinet 2005;20:268–74.
[8] Pfrunder A, Gutmann H, Beglinger C, Drewe J. Gene expression of CYP3A4, ABC-transporters (MDR1 and MRP1–MRP5) and hPXR in three different human colon carcinoma cell lines. J Pharm Pharmacol 2003;55:59–66.
[9] Thummel KE, Brimer C, Yasuda K, Thottassery J, Senn T, Lin Y, et al. Transcriptional control of intestinal cytochrome P-4503A by 1alpha,25-dihydroxy vitamin D3. Mol Pharmacol 2001;60:1399–406.
[10] Patel J, Pal D, Vangal V, Gandhi M, Mitra AL. Transport of HIV-protease inhibitors across 1 alpha,25di-hydroxy vitamin D3-treated Calu-3 cell monolayers: modulation of P-glycoprotein activity. Pharm Res 2002;19:1696–703.
[11] Piwnica-Worms D, Chiu ML, Budding M, Kronauge JF, Kramer RA, Croop JM. Functional imaging of multidrug-resistant P-glycoprotein with an organotechnetium complex. Cancer Res 1993;53:977–84.
[12] Yamaguchi S, Yachiku S, Hashimoto H, Kaneko S, Nishihara M, Niibori D, et al. Relation between technetium 99m-methoxyisobutylisonitrile accumulation and multidrug resistance protein in the parathyroid glands. World J Surg 2002;26:29–34.
[13] Olaizola I, Zingraff J, Heuguerot C, Fajardo L, Leger A, Lopez J, et al. [(99m)Tc]-sestamibi parathyroid scintigraphy in chronic haemodialysis patients: static and dynamic explorations. Nephrol Dial Transplant 2000;15:1201–6.
[14] Drocourt L, Ourlin JC, Pascussi JM, Maurel P, Vilarem MJ. Expression of CYP3A4, CYP2B6, and CYP2C9 is regulated by the vitamin D receptor pathway in primary human hepatocytes. J Biol Chem 2002;277:25125–32.
[15] Schrader M, Nayeri S, Kahlen JP, Muller KM, Carlberg C. Natural vitamin D3 response elements formed by inverted palindromes: polarity-directed ligand sensitivity of vitamin D3 receptor-retinoid X receptor heterodimer-mediated transactivation. Mol Cell Biol 1995;15:1154–61.
[16] Tavera-Mendoza L, Wang TT, Lallemant B, Zhang R, Nagai Y, Bourdeau V, et al. Convergence of vitamin D and retinoic acid signalling at a common hormone response element. EMBO Rep 2006;7:180–5.
[17] Matilainen M, Malinen M, Saavalainen K, Carlberg C. Regulation of multiple insulin-like growth factor binding protein genes by 1alpha,25-dihydroxyvitamin D3. Nucleic Acids Res 2005;33:5521–32.
[18] Seoane S, Perez-Fernandez R. The vitamin D receptor represses transcription of the pituitary transcription factor Pit-1 gene without involvement of the retinoid X receptor. Mol Endocrinol 2006;20:735–48.
[19] Kurose K, Saeki M, Tohkin M, Hasegawa R. Thyroid hormone receptor mediates human MDR1 gene expression—identification of the response region essential for gene expression. Arch Biochem Biophys 2008;474: 82–90.
[20] Nakamura T, Sakaeda T, Ohmoto N, Tamura T, Aoyama N, Shirakawa T, et al. Real-time quantitative polymerase chain reaction for MDR1, MRP1, MRP2, and CYP3A-mRNA levels in Caco-2 cell lines, human duodenal enterocytes, normal colorectal tissues, and colorectal adenocarcinomas. Drug Metab Dispos 2002;30:4–6.
[21] Kurose K, Ikeda S, Koyano S, Tohkin M, Hasegawa R, Sawada J. Identification of regulatory sites in the human PXR (NR1I2) promoter region. Mol Cell Biochem 2006;281:35–43.
[22] Hochman JH, Chiba M, Nishime J, Yamazaki M, Lin JH. Influence of P-glycoprotein on the transport and metabolism of indinavir in Caco-2 cells expressing cytochrome P-450 3A4. J Pharmacol Exp Ther 2000;292: 310–8.
[23] Pascussi JM, Gerbal-Chaloin S, Drocourt L, Maurel P, Vilarem MJ. The expression of CYP2B6, CYP2C9 and CYP3A4 genes: a tangle of networks of nuclear and steroid receptors. Biochim Biophys Acta 2003;1619:243–53.
[24] Xie W, Barwick JL, Simon CM, Pierce AM, Safe S, Blumberg B, et al. Reciprocal activation of xenobiotic response genes by nuclear receptors SXR/PXR and CAR. Genes Dev 2000;14:3014–23.
[25] Lempiainen H, Molnar F, Macias Gonzalez M, Perakyla M, Carlberg C. Antagonist- and inverse agonist-driven interactions of the vitamin D receptor and the constitutive androstane receptor with corepressor protein. Mol Endocrinol 2005;19:2258–72.
[26] Toell A, Polly P, Carlberg C. All natural DR3-type vitamin D response elements show a similar functionality in vitro. Biochem J 2000;352(Pt 2):301–9.
[27] Kim S, Yamazaki M, Zella LA, Shevde NK, Pike JW. Activation of receptor activator of NF-kappaB ligand gene expression by 1,25-dihydroxyvitamin D3 is mediated through multiple long-range enhancers. Mol Cell Biol 2006;26:6469–86.
[28] Quack M, Carlberg C. Ligand-triggered stabilization of vitamin D receptor/retinoid X receptor heterodimer conformations on DR4-type response elements. J Mol Biol 2000;296:743–56.
[29] Kimmel-Jehan C, Jehan F, DeLuca HF. Salt concentration determines 1,25-dihydroxyvitamin D3 dependency of vitamin D receptor–retinoid X receptor–vitamin D-

responsive element complex formation. Arch Biochem Biophys 1997;341:75–80.
[30] Engman HA, Lennernas H, Taipalensuu J, Otter C, Leidvik B, Artursson P. CYP3A4, CYP3A5, and MDR1 in human small and large intestinal cell lines suitable for drug transport studies. J Pharm Sci 2001;90:1736–51.
[31] Shabahang M, Buras RR, Davoodi F, Schumaker LM, Nauta RJ, Evans SR. 1,25-Dihydroxyvitamin D3 receptor as a marker of human colon carcinoma cell line differentiation and growth inhibition. Cancer Res 1993;53:3712–8.
[32] Ebeling PR, Sandgren ME, DiMagno EP, Lane AW, DeLuca HF, Riggs BL. Evidence of an age-related decrease in intestinal responsiveness to vitamin D: relationship between serum 1,25-dihydroxyvitamin D3 and intestinal vitamin D receptor concentrations in normal women. J Clin Endocrinol Metab 1992;75:176–82.
[33] Kinyamu HK, Gallagher JC, Prahl JM, DeLuca HF, Petranick KM, Lanspa SJ. Association between intestinal vitamin D receptor, calcium absorption, and serum 1,25 dihydroxyvitamin D in normal young and elderly women. J Bone Miner Res 1997;12:922–8.
[34] Bises G, Kallay E, Weiland T, Wrba F, Wenzl E, Bonner E, et al. 25-Hydroxyvitamin D3-1alpha-hydroxylase expression in normal and malignant human colon. J Histochem Cytochem 2004;52:985–9.
[35] Tangpricha V, Flanagan JN, Whitlatch LW, Tseng CC, Chen TC, Holt PR, et al. 25-Hydroxyvitamin D-1alpha-hydroxylase in normal and malignant colon tissue. Lancet 2001;357:1673–4.
[36] Walters JR, Balesaria S, Khair U, Sangha S, Banks L, Berry JL. The effects of Vitamin D metabolites on expression of genes for calcium transporters in human duodenum. J Steroid Biochem Mol Biol 2007;103:509–12.
[37] Dusso AS, Brown AJ, Slatopolsky E. Vitamin D. Am J Physiol Renal Physiol 2005;289:F8–28.
[38] Hewison M, Burke F, Evans KN, Lammas DA, Sansom DM, Liu P, et al. Extra-renal 25-hydroxyvitamin D3-1alpha-hydroxylase in human health and disease. J Steroid Biochem Mol Biol 2007;103:316–21.
[39] Kong J, Zhang Z, Musch MW, Ning G, Sun J, Hart J, et al. Novel role of the vitamin D receptor in maintaining the integrity of the intestinal mucosal barrier. Am J Physiol Gastrointest Liver Physiol 2008;294:G208–16.
[40] Kutuzova GD, DeLuca HF. 1,25-Dihydroxyvitamin D3 regulates genes responsible for detoxification in intestine. Toxicol Appl Pharmacol 2007;218:37–44.

0090-9556/10/3802-215–222$20.00
DRUG METABOLISM AND DISPOSITION
Copyright © 2010 by The American Society for Pharmacology and Experimental Therapeutics
DMD 38:215–222, 2010

Vol. 38, No. 2
30254/3548264
Printed in U.S.A.

Investigation of the Rate-Determining Process in the Hepatic Elimination of HMG-CoA Reductase Inhibitors in Rats and Humans

Takao Watanabe, Hiroyuki Kusuhara, Kazuya Maeda, Hiroshi Kanamaru, Yoshikazu Saito, Zhuohan Hu, and Yuichi Sugiyama

Laboratory of Molecular Pharmacokinetics, Graduate School of Pharmaceutical Sciences, The University of Tokyo, Tokyo, Japan (T.W., H.Ku., K.M., Y.Su.); Sumika Chemical Analysis Service, Ltd., Osaka, Japan (H.Ka., Y.Sa.); and Research Institute for Liver Diseases (Shanghai) Co. Ltd., Shanghai, China (Z.H.)

Received September 16, 2009; accepted October 23, 2009

ABSTRACT:

Elucidation of the rate-determining process in the overall hepatic elimination of drugs is critical for predicting their intrinsic hepatic clearance and the impact of variation of sequestration clearance on their systemic concentration. The present study investigated the rate-determining process in the overall hepatic elimination of the HMG-CoA reductase inhibitors pravastatin, pitavastatin, atorvastatin, and fluvastatin both in rats and humans. The uptake of these statins was saturable in both rat and human hepatocytes. Intrinsic hepatic clearance obtained by in vivo pharmacokinetic analysis in rats was close to the uptake clearance determined by the multiple indicator dilution method but much greater than the intrinsic metabolic clearance extrapolated from an in vitro model using liver microsomes. In vivo uptake clearance of the statins in humans (pravastatin, 1.44; pitavastatin, 30.6; atorvastatin, 12.7; and fluvastatin, 62.9 ml/min/g liver), which was obtained by multiplying in vitro uptake clearance determined in cryopreserved human hepatocytes by rat scaling factors, was within the range of overall in vivo intrinsic hepatic clearance (pravastatin, 0.84–1.2; pitavastatin, 14–35; atorvastatin, 11–19; and fluvastatin, 123–185 ml/min/g liver), whereas the intrinsic metabolic clearance of atorvastatin and fluvastatin was considerably low compared with their intrinsic hepatic clearance. Their uptake is the rate-determining process in the overall hepatic elimination of the statins in rats, and this activity likely holds true for humans. In vitro-in vivo extrapolation of the uptake clearance using a cryopreserved human hepatocytes model and rat scaling factors will be effective for predicting in vivo intrinsic hepatic clearance involving active uptake.

Predicting the pharmacokinetic properties of drug candidates in preclinical stages of development has been a critical issue for avoiding failure in clinical stages of development because of pharmacokinetics. The liver is the major clearance organ for drugs in the body where the inactivation mechanisms are composed of metabolic enzymes and drug transporters. These inactivation mechanisms are associated with the hepatic first-pass effect after oral administration and with elimination from the systemic circulation. It is well accepted that, because of large species differences in drug metabolism, the results of animal studies cannot be directly extrapolated to humans. Instead, in vitro systems have been developed to replace animal studies and provide reliable predictions. In particular, human liver microsomes enable the reliable prediction of the metabolic clearance of drugs in the liver of humans (Iwatsubo et al., 1997; Obach, 1999; Naritomi et al., 2001; Stringer et al., 2008; Kilford et al., 2009). It has been found that the substrates of hepatic uptake transporters, organic anion-transporting polypeptide (OATP) 1B1 and OATP1B3, include anionic drugs whose major elimination pathway is metabolism by cytochrome P450 (P450) and UDP-glucuronosyltransferase in the liver. These drugs include cerivastatin, atorvastatin, fluvastatin, repaglinide, and telmisartan (Fischer et al., 1999; Jacobsen et al., 2000; Bidstrup et al., 2003; Kirchheiner et al., 2003; Shitara and Sugiyama, 2006). These drugs have been considered as outliers in the prediction of elimination using human liver microsomes because of active transport in their uptake process, concentrating substrate drugs inside the cells.

For these drugs, the impact of variation of sequestration clearance on the drug concentrations in the systemic circulation depends on a rate-determining process (Kusuhara and Sugiyama, 2009). Despite its

This work was supported by a research grant (Development of Technology to Create Research Model Cells) from the New Energy and Industrial Technology Development Organization of Japan; and Health and Labour Sciences Research Grants for Research on Regulatory Science of Pharmaceuticals and Medical Devices from Ministry of Health, Labour and Welfare, Japan.

Article, publication date, and citation information can be found at http://dmd.aspetjournals.org.

doi:10.1124/dmd.109.030254.

ABBREVIATIONS: OATP, organic anion-transporting polypeptide; P450, cytochrome P450; statin, HMG-CoA reductase inhibitor; BCRP, breast cancer resistance protein; MID, multiple indicator dilution; R-122798, (3*R*,5*R*)-3,5-dihydroxy-7-[(1*S*,2*S*,6*S*,8*S*,8a*R*)-6-hydroxy-8-(isobutyryloxy)-2-methyl-1,2,6,7,8,8a-hexahydronaphthalen-1-yl]heptanoic acid; FD-4, fluorescein isothiocyanate dextran 4000; SD, Sprague-Dawley; LC/MS/MS, liquid chromatography/tandem mass spectrometry; AUC_{buf}^{0-t}, area under the statin concentrations in the incubation buffer; X_{hep}, amount of statin uptake into hepatocytes per 10^6 viable cells; C_{buf}, buffer concentration; BSA, bovine serum albumin; K_1, influx rate constant; $PS_{inf,MID}$, unbound uptake clearance; R_B, blood-to-plasma concentration ratio; f_B, unbound fraction in blood; AUC_P, area under the plasma concentration-time curve; $CL_{tot,B}$, total blood clearance; CL_H, hepatic clearance; F_H, hepatic availability; $CL_{int,all}$, overall intrinsic clearance; F_a, fraction absorbed.

importance for predicting the impact of variation of metabolic activity or canalicular efflux on systemic exposure, there are only a few studies examining the rate-determining process for the hepatic elimination of pravastatin and methotrexate in rats (Yamazaki et al., 1996; Ueda et al., 2001). Because of the lack of information regarding liver concentrations of these drugs, the rate-determining process in their overall hepatic elimination has not been investigated in humans. We proposed an in vitro-in vivo extrapolation in which the uptake clearance is extrapolated from an in vitro model using cryopreserved human hepatocytes and rat scaling factor based on the finding that scaling factors for P450-mediated metabolism are preserved across the species (Naritomi et al., 2001). The extrapolated uptake clearance of pravastatin was within the range of clinically reported intrinsic hepatic clearance, suggesting that the uptake is also the rate-determining process in humans (Watanabe et al., 2009). The purpose of this study was to apply this method to the other HMG-CoA reductase inhibitors (statins), pitavastatin, atorvastatin, and fluvastatin, in rats and humans. Hepatic elimination is the major pathway for elimination of these statins from the systemic circulation, but the mechanisms involved are different: atorvastatin and fluvastatin are metabolized by CYP3A4 and CYP2C9, respectively, and pitavastatin undergoes biliary excretion by breast cancer resistance protein (BCRP) (Fischer et al., 1999; Jacobsen et al., 2000; Kirchheiner et al., 2003; Hirano et al., 2005). Hepatic uptake of pravastatin, pitavastatin, and atorvastatin involves a transporter, OATP1B1, based on a kinetic analysis of pitavastatin using human hepatocytes (Hirano et al., 2004) and clinical studies for pravastatin, pitavastatin, and atorvastatin. Generic variation of OATP1B1, such as OATP1B1*5 and OATP1B1*15, shows reduced transport activities compared with the reference OATP1B1 (OATP1B1*1a) (Tirona et al., 2001; Iwai et al., 2004; Nozawa et al., 2005), and healthy volunteers carrying those genotypes exhibit greater systemic exposure of pravastatin, pitavastatin, and atorvastatin, indicating the importance of OATP1B1 in their hepatic uptake process (Nishizato et al., 2003; Maeda et al., 2006; Niemi et al., 2006; Ieiri et al., 2007; He et al., 2009). On the other hand, the systemic exposure of fluvastatin was independent of OATP1B1 genotype (Niemi et al., 2006), whereas fluvastatin is a substrate of OATP1B1 (Kopplow et al., 2005; Noé et al., 2007). OATP1B1 is suggested to only make a negligible contribution to the hepatic elimination of fluvastatin.

In the present study, the overall intrinsic hepatic clearances of the statins were determined from in vivo studies using rats, and their uptake clearances were determined using a multiple indicator dilution (MID) technique. Metabolic clearances were determined using liver microsomes. In addition, in vitro parameters for hepatic uptake and metabolism were determined using cryopreserved human hepatocytes and liver microsomes, and extrapolated to the corresponding in vivo parameters to compare these parameters with clinically determined intrinsic hepatic clearances. The present study suggests that hepatic uptake is the predominant factor for hepatic elimination of these representative statins.

Materials and Methods

Materials. Pravastatin and a pravastatin analog, R-122798, were donated by Daiichi Sankyo Co. (Tokyo, Japan). Pitavastatin was donated by Kowa Co. (Tokyo, Japan). Atorvastatin was purchased from AK Scientific (Mountain View, CA). Fluvastatin and cerivastatin were purchased from Toronto Research Chemicals Inc. (North York, ON, Canada). Fluorescein isothiocyanate dextran 4000 [(FD-4) 4000 Da] was purchased from Sigma-Aldrich (St. Louis, MO). All the other chemicals and reagents were of analytical grade and were readily available from commercial sources.

Animals. Male Sprague-Dawley (SD) rats (6–7 weeks old) were purchased from Nippon SLC (Shizuoka, Japan). All the animals were maintained under standard conditions with a reversed light/dark cycle and were treated humanely. Food and water were available ad libitum. The studies were conducted in accordance with the guidelines of the Institutional Animal Care Committee, Graduate School of Pharmaceutical Sciences, The University of Tokyo (Tokyo, Japan).

Preparation of Rat and Human Hepatocytes. Isolated rat hepatocytes were prepared from SD rats by the collagenase perfusion method described previously (Yamazaki et al., 1993). Isolated hepatocytes (viability >88%) were suspended in Krebs-Henseleit buffer, adjusted to 2.0×10^6 cells/ml, and stored on ice before the uptake experiment. Cryopreserved human hepatocytes were purchased from XenoTech LLC (Lenexa, KS), the Research Institute for Liver Disease (Shanghai, China), and In Vitro Technologies (Baltimore, MD). Just before the uptake experiment, the hepatocyte suspension was thawed at 37°C and poured into Tube A of the hepatocyte isolation kit (XenoTech LLC) containing supplemented Dulbecco's modified Eagle's medium and isotonic Percoll and then centrifuged (70*g*) for 5 min at 25°C. After the supernatant was removed, the cells were resuspended in 5 ml of supplemented Dulbecco's modified Eagle's medium in Tube B of the hepatocyte isolation kit. The number of viable cells was then determined using trypan blue staining. The cell viability of human hepatocytes ranged from 75 to 97%. Subsequently, the cells were resuspended in the remaining medium from Tube B (approximately 40 ml) and then centrifuged (50*g*) for 3 min at 25°C, followed by removal of the supernatant. Finally, the cells were resuspended in the Krebs-Henseleit buffer at a density of 2.0×10^6 viable cells/ml for the uptake experiment.

Determination of Statin Uptake Clearance Using Hepatocytes. This experiment was performed as described previously with a minor modification (Hirano et al., 2004). Before the uptake studies, the cell suspensions were prewarmed at 37°C for 3 min. The uptake reaction was initiated by adding an equal volume of buffer-containing drugs to the hepatocyte suspension. After incubation at 37°C for 0.5, 1.5, and 2.5 min, the reaction was terminated by separating the cells from the substrate solution. For this purpose, an aliquot of 80 to 100 μl of incubation mixture was placed in a 0.4-ml centrifuge tube containing 50 μl of 5 M ammonium acetate under a 100-μl layer of oil mixture (density, 1.015, a mixture of silicone oil and mineral oil; Sigma-Aldrich), and subsequently the sample tubes were centrifuged for 15 s using a tabletop centrifuge (10,000*g*, MC-150; Tomy Seiko, Tokyo, Japan). During this process, hepatocytes passed through the oil layer into the aqueous solution. Tubes were frozen in liquid nitrogen immediately after centrifugation and stored at −30°C until quantification. An aliquot was taken from the upper media portion and quenched in methanol, and the cells were taken from the centrifuge tube and sonicated in a new tube, containing methanol, to disintegrate them. The samples were vortexed and centrifuged, and supernatants from both the media and cell portions were analyzed by liquid chromatography/tandem mass spectrometry (LC/MS/MS). The area under the statin concentrations in the incubation buffer (AUC_{buf}^{0-t}) was calculated using a trapezoidal method. The amount of statin uptake into hepatocytes per 10^6 viable cells (X_{hep}) normalized by the buffer concentration (C_{buf}) can be described by the following equation:

$$\frac{X_{hep}}{C_{buf}} = PS_{inf,vitro} \times \frac{AUC_{buf}^{0-t}}{C_{buf}} + V_0 \quad (1)$$

where $PS_{inf,vitro}$ and V_0 represent uptake clearance into hepatocytes and the initial distribution volume, respectively. Based on eq. 1, the $X_{hep}(t)/C_{buf}(t)$ value was plotted against the $AUC_{buf}^{0-t}/C_{buf}(t)$ value, and $PS_{inf,vitro}$ was determined as the initial slope of the plot and expressed as the in vitro uptake clearance (μl/min/10^6 cells). A physiological scaling factor of 1.2×10^8 cells/g liver was used for scaling up to the organ level (Iwatsubo et al., 1997).

In Vivo Pharmacokinetic Analysis in Rats. Male SD rats, weighing approximately 240 to 300 g, were used for these experiments. Under ether anesthesia, the femoral artery was cannulated with a polyethylene catheter (SP-31; Natsume Seisakusho Co., Tokyo, Japan) for the collection of blood samples. The bile duct was cannulated with a polyethylene catheter (PE-10; Natsume Seisakusho Co.) for bile collection, and the bladder was cannulated with a silicon catheter to collect urine. The femoral vein was cannulated with a polyethylene catheter (SP-31; Natsume Seisakusho Co.) for the administration of statins. Each rat was placed in a Bollman cage and allowed to recover from the anesthesia before the experiments were continued. The rats were given statins intravenously at 1 μmol/kg (pitavastatin and atorvastatin) or 0.5 μmol/kg (fluvastatin). Blood samples were collected at the designated times

and centrifuged at 1500*g* for 10 min at 4°C to obtain plasma. Bile and urine samples were collected in preweighed test tubes at the designated intervals throughout the experiment. All the samples were stored at −30°C until quantification. Plasma, bile, and urine samples were deproteinized with two volumes of methanol and centrifuged at 15,000*g* for 10 min at 4°C. The supernatant was subjected to LC/MS/MS analysis.

Liver Perfusion Study (Multiple Indicator Dilution Method). The procedures are basically as reported (Miyauchi et al., 1993; Akita et al., 2002). Under ether anesthesia, the portal and hepatic veins were cannulated to allow infusion of the perfusate and to allow the outflow to be collected, respectively. The perfusate consisted of 3% bovine serum albumin (BSA) in the Krebs-Ringer bicarbonate buffer, pH 7.4, and the flow rate was 30 ml/min. After the stabilization period of 10 min, 200 μl of the perfusion solution containing FD-4 (100 μM), an extracellular reference, and each statin (50 μM) was administered as a bolus into the portal vein. After administration, the total effluent from the hepatic venous vein was collected at 1-s intervals for 10 s. The concentration of FD-4 and statins in the collected samples was determined using a fluorescence plate reader (485 nm for excitation and 520 nm for emission, FluoStar Optima; BMG Labtech GmbH, Offenburg, Germany) and by LC/MS/MS, respectively. The natural logarithm of the ratio of FD-4 to statin concentration in the outflow was plotted as a function of time. The initial slope of this plot, calculated by linear regression analysis using initial four to five data points, reflects the influx rate constant (K_1). The unbound uptake clearance ($PS_{inf,MID}$) can be calculated by the following equation (eq. 2):

$$f_u \times PS_{inf,MID} = K_1 \times V_{ext} \quad (2)$$

where f_u and V_{ext} represent the unbound fraction of statins in the perfusion buffer containing BSA and the extracellular volume, which can be estimated by multiplying the perfusate flow rate by the transit time of the extracellular reference, respectively.

Determination of the Metabolic Clearance of Statins Using Liver Microsomes. Rat liver microsomes were prepared from four rats using standard procedures and stored at −80°C until use, and human liver microsomes were purchased from XenoTech LLC. Each statin was incubated with a reaction mixture consisting of liver microsomes (final concentration, 1 mg/ml) and an NADPH-generating system (0.8 mM $NADP^+$, 8 mM glucose 6-phosphate, 1 U/ml glucose-6-phosphate dehydrogenase, and 3 mM $MgCl_2$) in the presence of 100 mM phosphate buffer, pH 7.4. After preincubation at 37°C for 5 min, each statin (final concentration, 0.1 μM) was added to initiate the enzyme reaction. The reaction was terminated at the following time points by mixing the reaction mixture with a 4-fold volume of methanol, followed by centrifugation at 15,000*g* for 10 min at 4°C. The time points when the reaction was terminated were 0, 5, 15, 30, and 60 min for the metabolic reaction of pitavastatin in rat microsomes; 0, 5, 15, 30, 60, 90, and 120 min for that in human microsomes; and 0, 5, 15, and 30 min for the metabolic reaction of atorvastatin and fluvastatin in rat and human microsomes. The metabolic reaction was continued until the fraction metabolized was greater than 15% so that we could obtain reliable parameters. The actual fractions metabolized at the end of experiment were 30, 25, and 34% (rat microsomes) and 23, 52, and 65% (human microsomes) for pitavastatin, atorvastatin, and fluvastatin, respectively.

The supernatant was subjected to LC/MS/MS analysis. The metabolic velocity was calculated as the slope of the natural log (concentration)-time plot. The in vitro intrinsic metabolic clearance ($CL_{met,int,vitro}$) was calculated by dividing initial metabolic velocity by the statin concentration in the incubation buffer corrected by the fraction unbound to liver microsomes. A physiological scaling factor of 44.8 mg protein/g liver (rats) or 48.8 mg protein/g liver (humans) was used for scaling up to the organ level (Naritomi et al., 2001).

Determination of Protein Binding. Binding of statins to plasma proteins, liver microsomes, or perfusion buffer containing BSA used in the MID study was determined by an ultrafiltration method. Rat plasma was obtained by the centrifugation of blood from male SD rats, and human serum was purchased from Cosmo Bio Co. (Tokyo, Japan). Each statin (final concentration; 5, 0.1, and 50 μM for plasma, microsome, and perfusate, respectively) was added to the protein solution and incubated at 37°C for 5 min. The specimen was applied to YM-30 Centrifree devices (Millipore Corporation, Billerica, MA), and the devices were centrifuged at 2000*g* for 5 min at 37°C. The fraction unbound was calculated as concentration found in filtrate per total concentration. The concentrations of the drugs in the filtrate and the protein solution before filtration were determined by LC/MS/MS. The adsorption of pravastatin, pitavastatin, and atorvastatin to the filter was negligible, and that of fluvastatin was 19%. The binding of fluvastatin was normalized with respect to the filter blank.

Determination of the Blood-to-Plasma Concentration Ratio. To determine the blood-to-plasma concentration ratio (R_B) values, blood was obtained from male SD rats. Statins (final concentration, 1 μM) were individually added to the blood samples, and they were incubated together at 37°C for 5 min. Plasma was prepared by centrifugation of the blood samples (1500*g*, 5 min). The concentrations of the statins in the plasma samples were determined by LC/MS/MS. R_B values in humans were cited from the previous studies (Tse et al., 1993; Lennernäs and Fager, 1997; FDA-approved package). The unbound fraction in the blood (f_B) was calculated by dividing the unbound fraction in plasma by R_B.

LC/MS/MS Analysis. The appropriate standard curves were prepared in the equivalent blank matrix and used for each analysis. High-concentration samples were diluted appropriately with blank matrix. R-122798 (for pravastatin and pitavastatin) and cerivastatin (for atorvastatin and fluvastatin) were used as analytical internal standards.

The LC/MS/MS system consisted of an Alliance 2795 separations module with an autosampler (Waters, Milford, MA) and a Micromass Quattro Ultima tandem quadrupole mass spectrometer with an electron ion spray interface (Waters). The desolvation gas (nitrogen) flow rate was 650 l/h; the cone gas (nitrogen) flow rate was 30 l/h; the source temperature was 150°C; and the desolvation temperature was 450°C.

It was operated in a multiple reaction monitoring mode using negative ion mode. Deprotonated molecular ions were formed using a capillary energy of 3.2 kV and cone energies of 50 V (pravastatin), 45 V (pitavastatin and cerivastatin), and 40 V (atorvastatin and fluvastatin). Product ions formed at collision energies of 12 eV (pravastatin, *m/z* 423.5→321.2; cerivastatin, *m/z* 458.5→396.1), 12 eV (pitavastatin, *m/z* 420.5→358.1; R-122798, *m/z* 409.5→321.2), 28 eV (atorvastatin, *m/z* 557.6→397.2), and 15 eV (fluvastatin, 410.3→348.2) were monitored. The mobile phase used for high-performance liquid chromatography was 0.1% formic acid/acetonitrile = 73:27 (for pravastatin and pitavastatin) or 55:45 (for atorvastatin and fluvastatin), and the flow rate was 0.4 ml/min. Chromatographic separation was achieved on a C18 column (Capcell Pak C18 MG-II column, 50 × 2 mm; particle size, 3 μm; Shiseido, Tokyo, Japan).

Eight-point calibration curves were generated by plotting the peak area ratios of analyte/internal standard against the nominal analyte concentrations using linear regression with $1/(\text{area ratio})^2$ weighting. The typical *R*-squared value of the calibration curves was 0.997 to 0.999. The concentration range was 1 to 1000 nM for atorvastatin and 3 to 3000 nM for the other statins. The back-calculated concentrations of all the calibration standards were to be within 15% of their individual nominal concentrations (±20% at the lower limit of quantitation). Intraday and interday variability for the quantification of statins was less than 15%.

Pharmacokinetic Analysis in Rats. Pharmacokinetic parameters were calculated using noncompartmental analysis. Area under the plasma concentration-time curve (AUC_P) was calculated using the trapezoidal rule with extrapolation to infinity, and total blood clearance ($CL_{tot,B}$) was estimated as dose/($AUC_P \times R_B$). $CL_{tot,B}$ was regarded as the hepatic clearance (CL_H) because the urinary excretion of all the statins in male SD rats was negligible. Hepatic availability (F_H) of pitavastatin, atorvastatin, and fluvastatin was calculated from the following equation:

$$CL_H = Q_H \times (1 - F_H) \quad (3)$$

where Q_H represents the hepatic blood flow. F_H of pravastatin could not be estimated accurately from eq. 3 because CL_H of pravastatin was hepatic blood flow-limited; in other words, F_H was extremely small. Therefore, F_H of pravastatin was obtained by dividing its bioavailability (Watanabe et al., 2009) by the fraction absorbed (Komai et al., 1992), assuming negligible metabolism in the small intestine. Overall intrinsic clearance ($CL_{int,all,vivo}$) was calculated from the following equations using a dispersion model (Roberts and Rowland, 1986).

$$F_H = \frac{4a}{(1+a)^2 \times \exp\{(a-1)/2/D_N\} - (1-a)^2 \times \exp\{-(a+1)/2/D_N\}} \quad (4)$$

$$a = (1 + 4R_N \times D_N)^{1/2} \quad (5)$$

$$R_N = f_B \times \frac{CL_{int,all,vivo}}{Q_H} \quad (6)$$

The hepatic blood flow rate was set at 50 to 80 ml/min/kg for rats and at 17 to 25.5 ml/min/kg for humans, and D_N was set at 0.17. A physiological scaling factor of 41.2 g liver/kg b.wt. (rats) or 24.1 g liver/kg b.wt. (humans) was used for scaling down to the organ level.

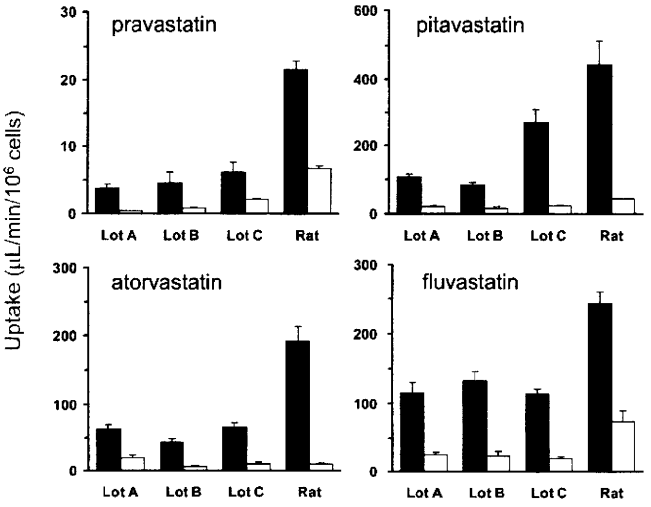

FIG. 1. Uptake clearance of statins in isolated human and rat hepatocytes. Uptake clearance of four statins by hepatocytes determined at 37°C at two concentrations (closed bar, 0.1 μM; open bar, 100 μM) by the oil filtration method. Cryopreserved human hepatocytes (three independent batches depicted as Lots A, B, and C) and freshly isolated rat hepatocytes were used in the determinations. Cells were incubated with statins for 0.5, 1.5, and 2.5 min; subsequently, reactions were terminated by rapid separation of the cells from the uptake buffer using centrifugation. The uptake is represented by the amount associated with the cell specimens divided by the statin concentrations in the uptake buffer. Data represent the mean ± S.E. (n = 3).

Pharmacokinetic Analysis in Humans. The availability in the liver (F_H) of pravastatin and atorvastatin was calculated using eq. 3 and the plasma concentration and urinary excretion data after intravenous administration in the clinical studies and f_B values (Singhvi et al., 1990; FDA-approved package). In the case of fluvastatin, F_{II} was calculated by dividing its bioavailability (0.33) by the fraction absorbed in humans (0.9) because its hepatic clearance (16 ml/min/kg) was close to the hepatic blood flow rate (Tse et al., 1992; Lindahl et al., 1996). F_{II} of pitavastatin was obtained from the following equation (eq. 7) using the plasma concentration data after oral administration in humans (Ando et al., 2005) and fraction absorbed (F_a) in rats (0.83) (Kimata et al., 1998), assuming no interspecies differences in F_a and negligible metabolism in the small intestine:

$$F_H = \frac{Q_H}{F_a \times CL_{oral} + Q_H} \quad (7)$$

where CL_{oral} is blood clearance after oral administration. Subsequently, $CL_{int,all,vivo}$ of each statin was calculated from eqs. 4 to 6.

Results

Uptake Clearances of Statins Determined Using Freshly Isolated Rat Hepatocytes and Cryopreserved Human Hepatocytes. The uptake clearances ($PS_{inf,vitro}$) of the statins were determined using rat and human hepatocytes (Fig. 1). The uptake clearance was markedly in the presence of excess amounts of the statins in both rat and human hepatocytes. $PS_{inf,vitro}$ determined at 0.1 μM are scaled up to the in vivo value per unit liver weight using the following physiological scaling factors: 41.2 g liver/kg, 1.2 × 10^8 cells/g liver for comparison with the corresponding $PS_{inf,MID}$. $PS_{inf,vitro}$ of statins in rats were almost similar or somewhat lower than $PS_{inf,MID}$ (Table 3).

Determination of the in Vivo Intrinsic Hepatic Clearance of Statins in Rats. Figure 2 shows time profiles of the plasma concentrations and the cumulative amount of statins excreted into the bile after intravenous administration. Approximately 50% of the dose was recovered in the bile after the administration of pitavastatin and atorvastatin, whereas fluvastatin was slightly excreted into the bile as unchanged form. Urinary excretion of all the statins was negligible. The pharmacokinetic parameters of the statins were determined by noncompartmental analysis (Table 1). The plasma/serum unbound fraction and R_B of each statin were also measured, and the findings are summarized in Table 2.

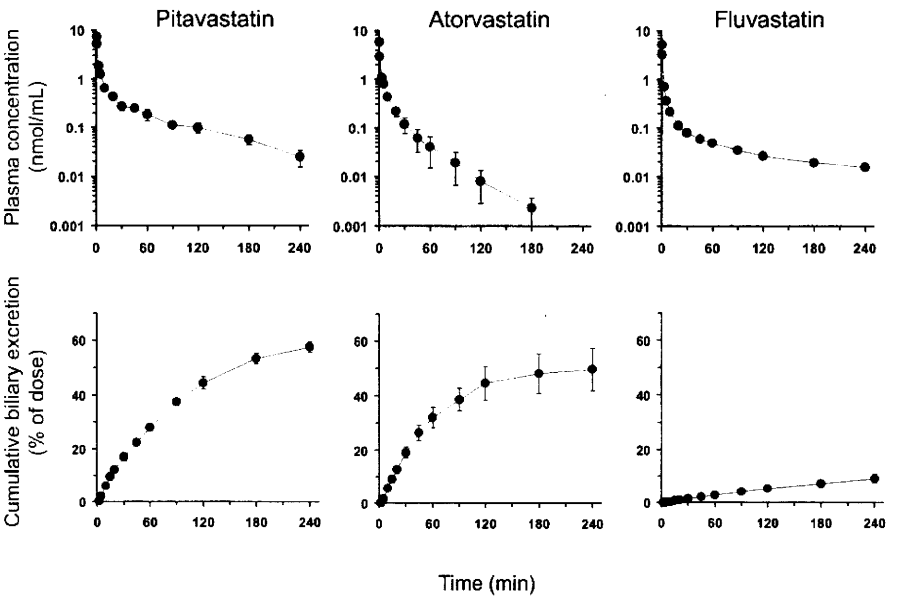

FIG. 2. Plasma concentration-time profiles (top) and cumulative biliary excretion (bottom) of statins after intravenous administration to male SD rats. Male SD rats were given statins: pitavastatin (1 μmol/kg, left), atorvastatin (1 μmol/kg, middle), and fluvastatin (0.5 μmol/kg, right), intravenously. The plasma concentrations were determined over 240 min after administration for pitavastatin, 180 min for atorvastatin, and 240 min for fluvastatin. Bile was collected from the common bile duct via an indwelling cannula, and the cumulative amount of biliary excretion was determined. Data represent the mean ± S.E. (n = 3).

TABLE 1

Pharmacokinetic parameters of statins in rats

	Dose	$CL_{tot,H}$	Biliary Excretion	Urinary Excretion	F_H
	μmol/kg	*ml/min/kg*	*% of dose*	*% of dose*	
Pravastatin[a]	0.5	62	43	<4	0.014
Pitavastatin	1	28	57	<0.1	0.44–0.65[b]
Atorvastatin	1	35	50	<0.1	0.29–0.56[b]
Fluvastatin	0.5	42	9	<0.1	0.17–0.48[b]

[a] Watanabe et al., 2009.
[b] Estimated from eq. 3 using Q_H (50–80 ml/min/kg).

Determination of the in Situ Intrinsic Hepatic Uptake Clearance of Statins. The intrinsic hepatic uptake clearance ($PS_{inf,MID}$) was determined by the multiple indicator dilution method using FD-4 as an extracellular space marker. The natural logarithm of the ratio of the concentration of FD-4 to that of each statin in the outflow (ratio plot) is given as a function of time in Fig. 3. The intrinsic hepatic uptake clearance ($PS_{inf,MID}$) of statins was determined from the slope of the plot and unbound fraction in the perfusate (Tables 2 and 3). For pitavastatin, to validate the unbound uptake clearance, $PS_{inf,MID}$ was determined using the perfusion buffers containing 1.5 or 3% BSA. The unbound fractions of pitavastatin in the presence of 1.5 and 3% BSA were 0.0859 and 0.0489, respectively, and $PS_{inf,MID}$ was similar [74.1 ± 25.1 and 91.5 ± 8.5 ml/min/g liver (mean ± S.E.), respectively].

Comparison of Intrinsic Clearances in the Hepatic Elimination of Statins by Rats. Intrinsic clearances related to the hepatic clearance of statins, such as $PS_{inf,MID}$, $PS_{inf,vitro}$, $CL_{met,int,vitro}$, and $CL_{int,all,vivo}$, by rats are summarized in Table 3. All the parameters were expressed as the value per unit weight of the liver. $CL_{int,all,vivo}$ was determined from eqs. 4 to 6 using F_H and f_B of each statin (Tables 1 and 2) and Q_H (1.21–1.94 ml/min/g liver). $PS_{inf,MID}$ and $PS_{inf,vitro}$ of statins were similar to $CL_{int,all,vivo}$, whereas $CL_{met,int,vitro}$ was much lower than $CL_{int,all,vivo}$ (Fig. 4).

Comparison of Intrinsic Clearances in the Hepatic Clearance of Statins by Humans. Intrinsic clearances of statins by humans are summarized in Table 4. All the parameters are expressed as the value per the unit weight of the liver except for the scaling factor. The uptake clearances determined by the in vitro model were extrapolated to in vivo clearances using physiological and drug-related scaling factors, and the latter scaling factor was defined as the ratio of the in situ to in vitro uptake clearances for each statin in rats. As observed in rats, the predicted uptake clearances ($PS_{inf,vivo,predicted}$) were similar to $CL_{int,all,vivo}$ obtained from the clinical studies. In contrast, the $CL_{met,int,vitro}$ of atorvastatin and fluvastatin was markedly low to account for $CL_{int,all,vivo}$ (Fig. 4), although these statins are mainly eliminated from the liver through metabolism by P450.

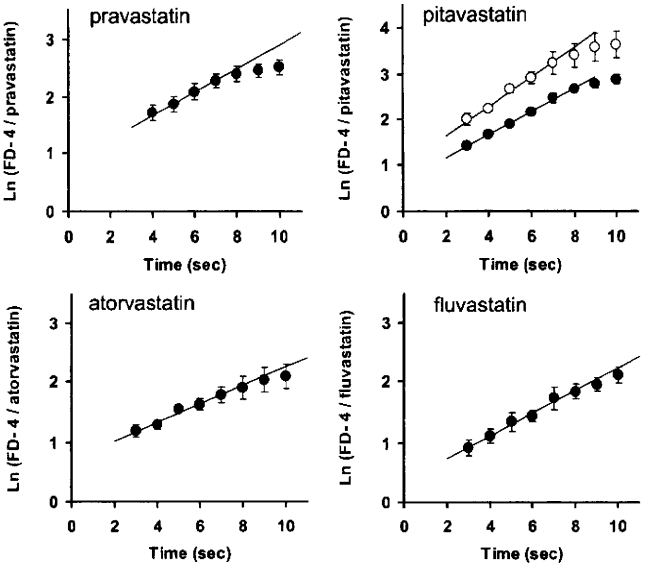

FIG. 3. Time profiles of the natural logarithm of the concentration ratio of FD-4 to statins in the outflow. After 10-min preperfusion, each statin (50 μM) and FD-4 (100 μM), an extracellular reference, were injected into the portal vein. After injection, the total effluent from the hepatic vein was collected at 1-s intervals for 10 s. For pitavastatin, the injected solution contained 3% (●) or 1.5% (○) BSA. Data represent the mean ± S.E. (n = 3).

Discussion

In a previous study, based on pharmacokinetic analyses, we proposed that the uptake is the rate-determining process in the overall hepatic elimination of pravastatin (Watanabe et al., 2009). The present study examined the rate-determining step in the overall hepatic elimination of other statins with different elimination mechanisms: biliary excretion for pitavastatin and P450-mediated metabolism for atorvastatin and fluvastatin.

Consistent with previous studies (Hirano et al., 2004), the uptake of pitavastatin by human hepatocytes was saturable (Fig. 1). In addition, uptake of atorvastatin and fluvastatin was also saturable in human hepatocytes (Fig. 1). Saturable uptake of atorvastatin is in good agreement with the clinical report in which coadministration of rifampicin, an inhibitor of OATP1B1, greatly enhanced the systemic exposure of atorvastatin, and the systemic exposure of atorvastatin is affected by the genotypes of OATP1B1 (Lau et al., 2007; He et al., 2009). Although an in vitro study using cDNA transfectants showed that fluvastatin is a substrate of OATP1B1 (Kopplow et al., 2005; Noé et al., 2007), the systemic exposure of fluvastatin was independent of the OATP1B1 genotypes (Niemi et al., 2006), suggesting that a transporter distinct from OATP1B1 may play a major role in the hepatic uptake of fluvastatin. An in vitro study using cDNA transfectants showed that fluvastatin is also a substrate of other hepatic uptake

TABLE 2

R_B and unbound fraction in the perfusion buffer, rat plasma, and human serum, as well as f_B for each statin

	Unbound Fraction					R_B		f_B	
	Perfusion Buffer	Rat Microsome	Human Microsome	Rat Plasma	Human Serum	Rat	Human[a]	Rat	Human
Pravastatin	0.683	N.D.	N.D.	0.676	0.554	0.59[b]	0.56	1.2	0.99
Pitavastatin	0.0489	0.418	0.432	0.0134	0.00523	0.65	0.58	0.021	0.0090
Atorvastatin	0.0817	0.557	0.405	0.0567	0.0511	1.2	0.61	0.047	0.084
Fluvastatin	0.0311	0.234	0.308	0.00986	0.00368	0.53	0.52	0.019	0.0071

N.D., not determined.
[a] Tse et al. (1993); Lennernas and Fager (1997); FDA-approved package.
[b] Yamazaki et al., 1996b.

TABLE 3

Intrinsic clearances of statins related to their hepatic clearance in rats

All the intrinsic clearances are scaled up to the in vivo clearance values per unit liver weight using the following physiological scaling factors: 41.2 g liver/kg, 1.2 × 10^8 cells/g liver, and 44.8 mg microsomal protein/g liver. Data represent the mean ± S.E. (n = 3).

	Uptake Clearance		Metabolic Clearance	Overall Intrinsic Clearance
	$PS_{inf,MID}$[a]	$PS_{inf,vitro}$[b]	$CL_{met,int,vitro}$[c]	$CL_{int,all,vivo}$[d]
	ml/min/g liver			
Pravastatin	6.48 ± 0.06	2.59 ± 0.14	0.793[e] ± 0.020	6.9–11
Pitavastatin	91.5 ± 8.5	53.3 ± 8.3	0.619 ± 0.434	42–53
Atorvastatin	42.1 ± 5.3	23.1 ± 2.5	0.910 ± 0.056	26–38
Fluvastatin	126 ± 12	29.2 ± 2.0	2.71 ± 0.24	85–154

[a] Determined by the MID analysis.
[b] Determined using rat hepatocytes at 0.1 μM.
[c] Determined using rat liver microsomes.
[d] Determined using the dispersion model with F_H, f_B, and Q_H (1.21–1.94 ml/min/g liver).
[e] Determined using rat liver S9 (Watanabe et al., 2009).

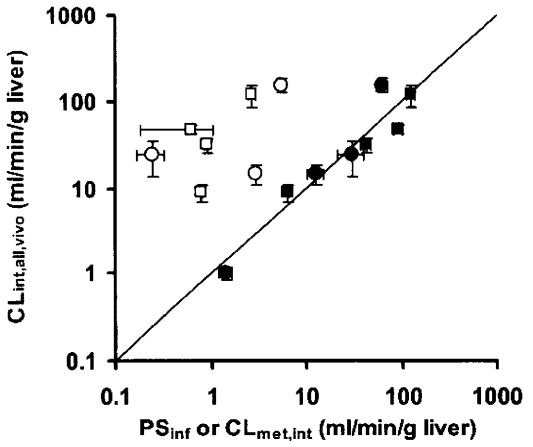

FIG. 4. Comparison of the hepatic overall intrinsic clearance of statins with the hepatic uptake clearance or metabolic clearance. In vivo hepatic overall intrinsic clearances of statins in rats and humans are plotted against the uptake clearance or metabolic clearance. ●, uptake clearance in humans predicted using scaling factor (Table 4); ○, metabolic clearance determined using human liver microsomes (Table 4); ■, uptake clearance in rats determined using a MID method (Table 3); □, metabolic clearance determined using rat liver microsomes (Table 3). The straight line indicates a 1:1 correlation. Each point represents the mean ± S.E. (n = 3).

transporters, such as OATP1B3 and OATP2B1 (Kopplow et al., 2005; Noé et al., 2007). As observed for other statins, variation of the uptake transport activities has a reciprocal relationship to the blood concentration of fluvastatin, and particularly, reduction of the uptake activity will increase the risk of an adverse reaction. Because of its negligible urinary excretion of fluvastatin, the variation in its hepatic uptake will have only a minimal impact on the liver concentration (Watanabe et al., 2009) and pharmacological response.

The rate-determining process was identified in rats by comparing the in vivo intrinsic hepatic clearance and uptake clearance. To obtain intrinsic hepatic clearance, the pharmacokinetics of pitavastatin, atorvastatin, and fluvastatin was examined in rats. Considering the recovery of the unchanged forms in the bile, biliary excretion and metabolism make a similar contribution to the intrinsic hepatic clearance of pitavastatin and atorvastatin, whereas hepatic metabolism is the predominant pathway for elimination of fluvastatin in rats. The uptake clearance ($PS_{inf,MID}$) of the statins was found to be similar to their corresponding intrinsic hepatic clearances ($CL_{int,all,vivo}$) (Table 3; Fig. 4). Namely, uptake is the rate-determining process in the hepatic elimination of the statins. In contrast, intrinsic sequestration clearances (metabolism for fluvastatin, biliary excretion and metabolism for atorvastatin and pitavastatin) were negligibly low accounting for the $CL_{int,all,vivo}$ (Table 3; Fig. 4). This poor predictability is likely the result of active uptake from the blood in the sinusoidal membrane.

The rate-determining process in the hepatic elimination of the statins was also examined in humans. In a previous study, we introduced the rat scaling factor to extrapolate in vitro uptake clearance of pravastatin determined using human hepatocytes to the in vivo clearance, which provided reasonable parameters to reproduce the plasma concentration-time profiles of pravastatin after intravenous and oral administration (Singhvi et al., 1990; Watanabe et al., 2009). In this study, we determined the scaling factor for each statin in rats by comparing their in situ and in vitro uptake clearances. The scaling factors of statins appear to be compound-dependent, ranging from 1.7 to 4.5 (Table 4). The scaling factor of the statins (pravastatin, atorvastatin, and pitavastatin), the hepatic uptake of which is mediated mainly by OATP1B1, is roughly 2, whereas that of fluvastatin, the hepatic uptake of which is mediated by the transporter distinct from OATP1B1, is 2-fold greater. Therefore, it can be speculated that the scaling factor is transporter-dependent. To support this speculation, accumulation of in vitro-in vivo extrapolation data for the transporters

TABLE 4

Intrinsic clearances regarding the hepatic clearance of statins in humans

All the intrinsic clearances are scaled up to the in vivo clearance values per unit liver weight using the following physiological scaling factors: 24.1 g liver/kg, 1.2 × 10^8 cells/g liver, and 48.8 mg microsomal protein/g liver. Data represent the mean ± S.E. (n = 3).

	Uptake Clearance			Metabolic Clearance	Overall Intrinsic Clearance
	$PS_{inf,vitro}$[a]	Scaling Factor[b]	$PS_{inf,vivo,predicted}$[c]	$CL_{met,int,vitro}$[d]	$CL_{int,all,vivo}$
	ml/min/g liver		*ml/min/g liver*	*ml/min/g liver*	
Pravastatin	0.575 ± 0.090	2.5 ± 0.1	1.44 ± 0.24	N.D.[e]	0.84–1.2[f]
Pitavastatin	18.5 ± 3.8	1.7 ± 0.3	30.6 ± 8.9	0.248 ± 0.081	14–35[g]
Atorvastatin	6.99 ± 0.55	1.8 ± 0.3	12.7 ± 2.3	2.98 ± 0.06	11–19[f]
Fluvastatin	14.5 ± 0.8	4.3 ± 0.5	62.9 ± 8.4	5.57 ± 0.28	123–185[h]

[a] Determined using human hepatocytes at 0.1 μM.
[b] Obtained from rats studies. These values were calculated by dividing $PS_{inf,MID}$ by $PS_{inf,vitro}$ in rats (Table 3).
[c] Calculated by multiplying $PS_{inf,vitro}$, determined using human hepatocytes by the corresponding scaling factor obtained in rats.
[d] Determined using human liver microsomes.
[e] No metabolism was detected in human S9 (Watanabe et al., 2009).
[f] Calculated from the plasma concentration and urinary excretion data after intravenous administration in the clinical studies (Singhvi et al., 1990; FDA-approved package).
[g] Calculated from the plasma concentration and urinary excretion data after oral administration in the clinical studies (Ando et al., 2005) and the fraction absorbed in rats (0.83) (Kimata et al., 1998). The details of this estimation are described in the text.
[h] Calculated from bioavailability and fraction absorbed in the clinical studies.

is absolutely essential. Because 1) the in vivo uptake clearance predicted for humans was in the range of $CL_{int,all,vivo}$ (Table 4) and 2) $CL_{met,int,vitro}$ of atorvastatin and fluvastatin determined using human liver microsomes was less than $CL_{int,all,vivo}$, uptake is the most likely rate-determining process in the hepatic elimination of the statins in humans. Lau et al. (2007) also suggested that hepatic uptake was important for systemic exposure of atorvastatin based on the clinical drug-drug interaction study between atorvastatin and a potent inhibitor of OATPs, rifampicin. Thus, impact of the variation of the sequestration clearance (metabolism or biliary excretion) caused by drug-drug interactions or genetic polymorphisms depends on the rate-determining process and will be smaller for these statins compared with drugs that achieve a rapid equilibrium. Indeed, the increase (2.5–3-fold) in the AUC of atorvastatin caused by concomitant use of itraconazole, a potent CYP3A4 inhibitor, was less remarkable than for other CYP3A4 substrates, such as midazolam and triazolam (5–10-fold increase) (Venkatakrishnan et al., 2000; Shitara and Sugiyama, 2006). BCRP genotypes produce no significant interindividual variation of the systemic exposure of pitavastatin (Ieiri et al., 2007), although they play a predominant role in mice (Hirano et al., 2005). It should be noted that, irrespective of the rate-determining process, the sequestration clearance is the predominant factor determining the liver concentration of the statins (Watanabe et al., 2009). Thus, inhibition of CYP3A4 or BCRP polymorphisms results in a significant increase in the liver concentration of atorvastatin and pitavastatin, respectively, leading to the enhancement of their pharmacological action. To validate the prediction of the rate-determining process of these statins, information regarding the tissue concentration-time profile is necessary. Clinical studies using positron emission tomography/single photon emission computed tomography will allow an advancement to improve the predictability of pharmacokinetic parameters.

To determine the intrinsic hepatic clearance that comprises uptake, sinusoidal efflux, and metabolism, Soars et al. (2007) proposed a "media loss" assay using isolated hepatocytes. Using this method, an intrinsic clearance can be determined from the concentration-time profile of drugs in incubation media and the initial amount of drugs applied. In theory, the method must be able to provide a reliable overall hepatic intrinsic clearance. However, as described in the report by Soars et al. (2007), this method considerably underestimates the in vivo overall intrinsic clearance (with an average 16-fold error), possibly because of reduced activities of transporters and/or enzymes during the relatively long-term incubation. Therefore, at present, separate determination of the uptake and metabolic clearances will provide more reliable parameters to predict the intrinsic hepatic clearance using rat scaling factors.

The present study found that the underestimation of in vivo intrinsic hepatic clearance of the statins in the in vitro-in vivo extrapolation of metabolic clearance is because of active transport in the uptake process. Kinetic analyses showed that uptake is the rate-determining process in the hepatic elimination of the statins in rats, which likely holds true in humans. In vitro-in vivo extrapolation of the uptake clearance using a human hepatocyte model and scaling factors determined in rats should be effective for predicting in vivo intrinsic hepatic clearance of drugs when transporter(s) are involved in the hepatic uptake.

Acknowledgments. We thank Toichiro Yamada and Ryoko Asaki for excellent technical assistance.

References

Akita H, Suzuki H, and Sugiyama Y (2002) Sinusoidal efflux of taurocholate correlates with the hepatic expression level of Mrp3. *Biochem Biophys Res Commun* **299:**681–687.

Ando H, Tsuruoka S, Yanagihara H, Sugimoto K, Miyata M, Yamazoe Y, Takamura T, Kaneko S, and Fujimura A (2005) Effects of grapefruit juice on the pharmacokinetics of pitavastatin and atorvastatin. *Br J Clin Pharmacol* **60:**494–497.

Bidstrup TB, Bjørnsdottir I, Sidelmann UG, Thomsen MS, and Hansen KT (2003) CYP2C8 and CYP3A4 are the principal enzymes involved in the human in vitro biotransformation of the insulin secretagogue repaglinide. *Br J Clin Pharmacol* **56:**305–314.

Fischer V, Johanson L, Heitz F, Tullman R, Graham E, Baldeck JP, and Robinson WT (1999) The 3-hydroxy-3-methylglutaryl coenzyme A reductase inhibitor fluvastatin: effect on human cytochrome P-450 and implications for metabolic drug interactions. *Drug Metab Dispos* **27:**410–416.

He YJ, Zhang W, Chen Y, Guo D, Tu JH, Xu LY, Tan ZR, Chen BL, Li Z, Zhou G, et al. (2009) Rifampicin alters atorvastatin plasma concentration on the basis of SLCO1B1 521T>C polymorphism. *Clin Chim Acta* **405:**49–52.

Hirano M, Maeda K, Matsushima S, Nozaki Y, Kusuhara H, and Sugiyama Y (2005) Involvement of BCRP (ABCG2) in the biliary excretion of pitavastatin. *Mol Pharmacol* **68:**800–807.

Hirano M, Maeda K, Shitara Y, and Sugiyama Y (2004) Contribution of OATP2 (OATP1B1) and OATP8 (OATP1B3) to the hepatic uptake of pitavastatin in humans. *J Pharmacol Exp Ther* **311:**139–146.

Ieiri I, Suwannakul S, Maeda K, Uchimaru H, Hashimoto K, Kimura M, Fujino H, Hirano M, Kusuhara H, Irie S, et al. (2007) SLCO1B1 (OATP1B1, an uptake transporter) and ABCG2 (BCRP, an efflux transporter) variant alleles and pharmacokinetics of pitavastatin in healthy volunteers. *Clin Pharmacol Ther* **82:**541–547.

Iwai M, Suzuki H, Ieiri I, Otsubo K, and Sugiyama Y (2004) Functional analysis of single nucleotide polymorphisms of hepatic organic anion transporter OATP1B1 (OATP-C). *Pharmacogenetics* **14:**749–757.

Iwatsubo T, Hirota N, Ooie T, Suzuki H, Shimada N, Chiba K, Ishizaki T, Green CE, Tyson CA, and Sugiyama Y (1997) Prediction of in vivo drug metabolism in the human liver from in vitro metabolism data. *Pharmacol Ther* **73:**147–171.

Jacobsen W, Kuhn B, Soldner A, Kirchner G, Sewing KF, Kollman PA, Benet LZ, and Christians U (2000) Lactonization is the critical first step in the disposition of the 3-hydroxy-3-methylglutaryl-CoA reductase inhibitor atorvastatin. *Drug Metab Dispos* **28:**1369–1378.

Kilford PJ, Stringer R, Sohal B, Houston JB, and Galetin A (2009) Prediction of drug clearance by glucuronidation from in vitro data: use of combined P450 and UGT cofactors in alamethicin activated human liver microsomes. *Drug Metab Dispos* **37:**82–89.

Kimata H, Fujino H, Koide T, Yamada Y, Tsunenari Y, and Yanagawa Y (1998) Studies on the metabolic fate of NK-104, a new inhibitor of HMG-CoA reductase (1): absorption, distribution, metabolism and excretion in rats. *Xenobiotic Metab Dispos* **13:**484–498.

Kirchheiner J, Kudlicz D, Meisel C, Bauer S, Meineke I, Roots I, and Brockmöller J (2003) Influence of CYP2C9 polymorphisms on the pharmacokinetics and cholesterol-lowering activity of (−)-3S,5R-fluvastatin and (+)-3R,5S-fluvastatin in healthy volunteers. *Clin Pharmacol Ther* **74:**186–194.

Komai T, Kawai K, Tokui T, Tokui Y, Kuroiwa C, Shigehara E, and Tanaka M (1992) Disposition and metabolism of pravastatin sodium in rats, dogs and monkeys. *Eur J Drug Metab Pharmacokinet* **17:**103–113.

Kopplow K, Letschert K, König J, Walter B, and Keppler D (2005) Human hepatobiliary transport of organic anions analyzed by quadruple-transfected cells. *Mol Pharmacol* **68:**1031–1038.

Kusuhara H and Sugiyama Y (2009) In vitro-in vivo extrapolation of transporter-mediated clearance in the liver and kidney. *Drug Metab Pharmacokinet* **24:**37–52.

Lau YY, Huang Y, Frassetto L, and Benet LZ (2007) Effect of OATP1B transporter inhibition on the pharmacokinetics of atorvastatin in healthy volunteers. *Clin Pharmacol Ther* **81:**194–204.

Lennernäs H and Fager G (1997) Pharmacodynamics and pharmacokinetics of the HMG-CoA reductase inhibitors. Similarities and differences. *Clin Pharmacokinet* **32:**403–425.

Lindahl A, Sandström R, Ungell AL, Abrahamsson B, Knutson TW, Knutson L, and Lennernäs H (1996) Jejunal permeability and hepatic extraction of fluvastatin in humans. *Clin Pharmacol Ther* **60:**493–503.

Maeda K, Ieiri I, Yasuda K, Fujino A, Fujiwara H, Otsubo K, Hirano M, Watanabe T, Kitamura Y, Kusuhara H, et al. (2006) Effects of organic anion transporting polypeptide 1B1 haplotype on pharmacokinetics of pravastatin, valsartan, and temocapril. *Clin Pharmacol Ther* **79:**427–439.

Miyauchi S, Sawada Y, Iga T, Hanano M, and Sugiyama Y (1993) Comparison of the hepatic uptake clearances of fifteen drugs with a wide range of membrane permeabilities in isolated rat hepatocytes and perfused rat livers. *Pharm Res* **10:**434–440.

Naritomi Y, Terashita S, Kimura S, Suzuki A, Kagayama A, and Sugiyama Y (2001) Prediction of human hepatic clearance from in vivo animal experiments and in vitro metabolic studies with liver microsomes from animals and humans. *Drug Metab Dispos* **29:**1316–1324.

Niemi M, Pasanen MK, and Neuvonen PJ (2006) SLCO1B1 polymorphism and sex affect the pharmacokinetics of pravastatin but not fluvastatin. *Clin Pharmacol Ther* **80:**356–366.

Nishizato Y, Ieiri I, Suzuki H, Kimura M, Kawabata K, Hirota T, Takane H, Irie S, Kusuhara H, Urasaki Y, et al. (2003) Polymorphisms of OATP-C (SLC21A6) and OAT3 (SLC22A8) genes: consequences for pravastatin pharmacokinetics. *Clin Pharmacol Ther* **73:**554–565.

Noé J, Portmann R, Brun ME, and Funk C (2007) Substrate-dependent drug-drug interactions between gemfibrozil, fluvastatin and other organic anion-transporting peptide (OATP) substrates on OATP1B1, OATP2B1, and OATP1B3. *Drug Metab Dispos* **35:**1308–1314.

Nozawa T, Minami H, Sugiura S, Tsuji A, and Tamai I (2005) Role of organic anion transporter OATP1B1 (OATP-C) in hepatic uptake of irinotecan and its active metabolite, 7-ethyl-10-hydroxycamptothecin: in vitro evidence and effect of single nucleotide polymorphisms. *Drug Metab Dispos* **33:**434–439.

Obach RS (1999) Prediction of human clearance of twenty-nine drugs from hepatic microsomal intrinsic clearance data: an examination of in vitro half-life approach and nonspecific binding to microsomes. *Drug Metab Dispos* **27:**1350–1359.

Roberts MS and Rowland M (1986) A dispersion model of hepatic elimination: 1. Formulation of the model and bolus considerations. *J Pharmacokinet Biopharm* **14:**227–260.

Shitara Y and Sugiyama Y (2006) Pharmacokinetic and pharmacodynamic alterations of 3-hydroxy-3-methylglutaryl coenzyme A (HMG-CoA) reductase inhibitors: drug-drug interactions and interindividual differences in transporter and metabolic enzyme functions. *Pharmacol Ther* **112:**71–105.

Singhvi SM, Pan HY, Morrison RA, and Willard DA (1990) Disposition of pravastatin sodium, a tissue-selective HMG-CoA reductase inhibitor, in healthy subjects. *Br J Clin Pharmacol* **29:**239–243.

Soars MG, Grime K, Sproston JL, Webborn PJ, and Riley RJ (2007) Use of hepatocytes to assess the contribution of hepatic uptake to clearance in vivo. *Drug Metab Dispos* **35:**859–865.

Stringer R, Nicklin PL, and Houston JB (2008) Reliability of human cryopreserved hepatocytes and liver microsomes as in vitro systems to predict metabolic clearance. *Xenobiotica* **38:**1313–1329.

Tirona RG, Leake BF, Merino G, and Kim RB (2001) Polymorphisms in OATP-C: identification of multiple allelic variants associated with altered transport activity among European- and African-Americans. *J Biol Chem* **276:**35669–35675.

Tse FL, Jaffe JM, and Troendle A (1992) Pharmacokinetics of fluvastatin after single and multiple doses in normal volunteers. *J Clin Pharmacol* **32:**630–638.

Tse FL, Nickerson DF, and Yardley WS (1993) Binding of fluvastatin to blood cells and plasma proteins. *J Pharm Sci* **82:**942–947.

Ueda K, Kato Y, Komatsu K, and Sugiyama Y (2001) Inhibition of biliary excretion of methotrexate by probenecid in rats: quantitative prediction of interaction from in vitro data. *J Pharmacol Exp Ther* **297:**1036–1043.

Venkatakrishnan K, von Moltke LL, and Greenblatt DJ (2000) Effects of the antifungal agents on oxidative drug metabolism: clinical relevance. *Clin Pharmacokinet* **38:**111–180.

Watanabe T, Kusuhara H, Maeda K, Shitara Y, and Sugiyama Y (2009) Physiologically based pharmacokinetic modeling to predict transporter-mediated clearance and distribution of pravastatin in humans. *J Pharmacol Exp Ther* **328:**652–662.

Yamazaki M, Akiyama S, Nishigaki R, and Sugiyama Y (1996) Uptake is the rate-limiting step in the overall hepatic elimination of pravastatin at steady-state in rats. *Pharm Res* **13:**1559–1564.

Yamazaki M, Suzuki H, Hanano M, Tokui T, Komai T, and Sugiyama Y (1993) Na(+)-independent multispecific anion transporter mediates active transport of pravastatin into rat liver. *Am J Physiol* **264:**G36–G44.

Address correspondence to: Yuichi Sugiyama, Laboratory of Molecular Pharmacokinetics, Graduate School of Pharmaceutical Sciences, The University of Tokyo, 7-3-1 Hongo, Bunkyoku-Tokyo, 113-0033, Japan. E-mail: sugiyama@mol.f.u-tokyo.ac.jp

0022-3565/09/3282-652–662$20.00
THE JOURNAL OF PHARMACOLOGY AND EXPERIMENTAL THERAPEUTICS
Vol. 328, No. 2
146647/3429080
Printed in U.S.A.

JPET 328:652–662, 2009

Physiologically Based Pharmacokinetic Modeling to Predict Transporter-Mediated Clearance and Distribution of Pravastatin in Humans

Takao Watanabe, Hiroyuki Kusuhara, Kazuya Maeda, Yoshihisa Shitara, and Yuichi Sugiyama

Department of Molecular Pharmacokinetics, Graduate School of Pharmaceutical Sciences, The University of Tokyo, Tokyo, Japan (T.W., H.K., K.M., Y.Su.); and Department of Biopharmaceutics, Graduate School of Pharmaceutical Sciences, Chiba University, Chiba, Japan (Y.Sh.)

Received September 25, 2008; accepted November 7, 2008

ABSTRACT

Hepatobiliary excretion mediated by transporters, organic anion-transporting polypeptide (OATP) 1B1 and multidrug resistance-associated protein (MRP) 2, is the major elimination pathway of an HMG-CoA reductase inhibitor, pravastatin. The present study examined the effects of changes in the transporter activities on the systemic and liver exposure of pravastatin using a physiologically based pharmacokinetic model. Scaling factors, determined by comparing in vivo and in vitro parameters of pravastatin in rats for the hepatic uptake and canalicular efflux, were obtained. The simulated plasma and liver concentrations and biliary excretion profiles were very close to the observed data in rats under linear and nonlinear conditions. In vitro parameters, determined in human cryopreserved hepatocytes and canalicular membrane vesicles, were extrapolated to in vivo parameters using the scaling factors obtained in rats. The simulated plasma concentrations of pravastatin were close to the reported values in humans. Sensitivity analyses showed that changes in the hepatic uptake ability altered the plasma concentration of pravastatin markedly but had a minimal effect on the liver concentration, whereas changes in the ability of canalicular efflux altered the liver concentration of pravastatin markedly but had a small effect on the plasma concentration. In conclusion, the model allows the prediction of the disposition of pravastatin in humans. The present study suggests that changes in the OATP1B1 activities may have a small and a large impact on the therapeutic efficacy and side effect (myopathy) of pravastatin, respectively, whereas those in the MRP2 activities may have opposite impacts (i.e., large and small impacts on the therapeutic efficacy and side effect).

Predicting the disposition of drugs in humans, particularly in the early stages of drug development, has been a critical issue in selecting the proper candidate drugs because the exposure of drugs to target organs is the major factor determining their pharmacological and/or toxicological activity. Human liver microsomes allow the reliable prediction of the metabolic clearance of drugs in humans (Rane et al., 1977; Iwatsubo et al., 1997; Obach, 1999; Naritomi et al., 2001). Biliary excretion, another hepatic elimination pathway, is the major systemic elimination pathway, particularly for amphipathic anionic drugs such as HMG-CoA reductase inhibitors (statins) and angiotensin II receptor antagonists. Because multiple transporters on the sinusoidal and canalicular membranes are involved, it is necessary to separately determine three kinetic parameters: 1) uptake, 2) sinusoidal efflux, and 3) canalicular efflux, to predict biliary clearance with regard to the plasma concentration (Giacomini and Sugiyama, 2005; Shitara et al., 2006a). The uptake clearance determined in freshly isolated rat hepatocytes correlates well with that determined with the multiple indicator dilution method (Miyauchi et al., 1993), and rat hepatocytes are reported to be a useful tool for predicting the hepatic clearance of drugs with significant hepatic uptake (Soars et al., 2007). Although cryopreserved human hepatocytes and canalicular membrane vesicles (CMVs) are commercially available, their usefulness in predicting in vivo hepatic up-

Article, publication date, and citation information can be found at http://jpet.aspetjournals.org.
doi:10.1124/jpet.108.146647.

ABBREVIATIONS: CMV, canalicular membrane vesicle; PBPK, physiologically based pharmacokinetic; OATP, organic anion-transporting polypeptide; MRP, multidrug resistance-associated protein; SF, scaling factor; R-122798, (3*R*,5*R*)-3,5-dihydroxy-7-[(1*S*,2*S*,6*S*,8*S*,8a*R*)-6-hydroxy-8-(isobutyryloxy)-2-methyl-1,2,6,7,8,8a-hexahydronaphthalen-1-yl]heptanoic acid; LC/MS, liquid chromatography/mass spectrometry; PS, permeability surface product; inf, influx; dif, diffusion; CL, clearance; met, metabolism; tot, total; B, blood; AUC, area(s) under the concentration-time curve.

take and canalicular efflux clearance remains to be examined. No method to quantify in vitro sinusoidal efflux has yet been established.

A physiologically based pharmacokinetic (PBPK) model, in which compartments representing tissues are connected with the blood flow, has been used to predict the time profiles of plasma and tissue concentrations (Kawai et al., 1998; Jones et al., 2006). The PBPK model is quite useful for simulating the effects of drug-drug interactions and genetic variations in drug-metabolizing enzymes and transporters on the exposure of drugs to the blood and organs and, ultimately, their effects on the pharmacological actions of drugs (Jones et al., 2006; Shitara and Sugiyama, 2006a). The purpose of this study was to establish a PBPK model to describe the disposition of pravastatin for which transporters are deeply involved in its hepatobiliary transport. Pravastatin, one of the statins used for the treatment of hyperlipidemia, was selected as the model compound in this study. The liver is a target organ for the pharmacological actions of statins, whereas myotoxic adverse effects, sometimes severe, including myopathy or rhabdomyolysis, are associated with the use of statins. Therefore, it is very important to simulate the exposure of statins to the liver and skeletal muscle to predict their pharmacological and toxicological effects. Hepatobiliary transport is the main elimination pathway of pravastatin from the systemic circulation and is mediated by uptake and efflux transporters in the liver (Shitara and Sugiyama, 2006b). The hepatic uptake of pravastatin is mainly mediated by organic anion-transporting polypeptide (OATP) 1B1, and its biliary excretion is predominantly mediated by multidrug resistance-associated protein (MRP) 2 (Yamazaki et al., 1993, 1997; Nakai et al., 2001). Pravastatin undergoes urinary excretion by tubular secretion and by glomerular filtration in humans (Singhvi et al., 1990). Organic anion transporter 3 has been suggested to be responsible for the basolateral uptake of pravastatin in rats and humans (Hasegawa et al., 2002; Nakagomi-Hagihara et al., 2007), whereas the transporter involved in its luminal efflux is yet to be identified.

In this study, in vivo experiments were carried out using male rats to obtain concentration-time profiles of pravastatin in the plasma, liver, kidney, muscle, brain, and lung. The kinetic parameters for the hepatic uptake and canalicular efflux of pravastatin were determined from in vitro transport studies using freshly isolated rat hepatocytes and CMVs, respectively. In vitro-in vivo scaling factors (SFs) were obtained for the hepatic uptake and subsequent canalicular efflux of pravastatin in rats. A PBPK model was constructed to simulate the systemic and liver exposure of pravastatin in rats. Using the PBPK model, the SFs determined in rats and kinetic parameters determined using human materials, the plasma concentration-time curve of pravastatin in humans was also simulated. Finally, the effects of changes in these transporter activities, caused by genetic polymorphisms and drug-drug interactions, on the concentration profiles of pravastatin in plasma and the liver were examined using the PBPK model.

Materials and Methods

Materials

[^{3}H]Pravastatin (45.5 Ci/mmol), unlabeled pravastatin, and a pravastatin analog, R-122798, were provided by Daiichi Sankyo Co., Ltd. (Tokyo, Japan). Cryopreserved human hepatocytes and human liver S9 fractions were purchased from In Vitro Technologies (Baltimore, MD). Human liver S9 fractions were also purchased from XenoTech, LLC (Lenexa, KS) and Tissue Transformation Technology (Edison, NJ). All other chemicals and reagents were of analytical grade and were readily available from commercial sources.

Animals

Male Sprague-Dawley rats (6–7 weeks old) were purchased from Nippon SLC (Hamamatsu, Japan). All animals were maintained under standard conditions with a reversed light/dark cycle and were treated humanely. Food and water were available ad libitum. The studies were carried out in accordance with the guidelines of the Institutional Animal Care Committee, Graduate School of Pharmaceutical Sciences, The University of Tokyo, Tokyo, Japan.

Animal Experiments

Male Sprague-Dawley rats, weighing approximately 250 to 320 g, were used throughout the experiments. Under ether anesthesia, the femoral artery was cannulated with a polyethylene catheter (SP-31) for the collection of blood samples. The bile duct was cannulated with a polyethylene catheter (PE-10) for bile collection, and the bladder was cannulated with a silicon catheter to collect urine. The femoral vein or the duodenum was cannulated with a polyethylene catheter (SP-31) for the administration of pravastatin. Each rat was placed in a Bollman cage and allowed to recover from the anesthesia before the experiments were continued. The rats were given pravastatin intravenously at 0.2, 1, 10, 50, or 200 mg/kg or intraduodenally at 20 mg/kg. Blood samples were collected at the designated times and centrifuged at 1500*g* for 10 min at 4°C to obtain plasma. Bile and urine samples were collected in preweighed test tubes at the designated intervals throughout the experiment. After the last blood sample had been taken, each rat was killed, and the liver, kidney, brain, lungs, and skeletal muscle were excised immediately for the tissue distribution study. The tissues were weighed and flash frozen in liquid nitrogen. All the samples were stored at −20°C until quantification.

Transport Study Using Human Cryopreserved Hepatocytes

This experiment was performed as described previously (Shitara et al., 2003). In brief, immediately before the study, the hepatocytes were thawed at 37°C. After they had been washed twice with ice-cold Krebs-Henseleit buffer, the cells were resuspended in Krebs-Henseleit buffer to a cell density of 1.0×10^6 viable cells/ml for the uptake study. After preincubation of the cells (1.2×10^5 cells/reaction) at 37°C for 3 min, drug uptake was initiated by the addition of labeled and unlabeled substrates to the cell suspension. The reaction was terminated after 0.5 or 2 min by separating the cells from the substrate solution. For this purpose, an aliquot of 100 μl of incubation mixture was placed in a centrifuge tube (450 μl) containing 50 μl of 2 N NaOH under a layer of 100 μl of oil (density = 1.015, a mixture of silicone oil and mineral oil; Sigma-Aldrich, St. Louis, MO). The sample tube was centrifuged for 10 s in a tabletop centrifuge (10,000*g*; Beckman Microfuge E; Beckman Coulter, Fullerton, CA). After overnight incubation in alkali to dissolve the hepatocytes, the centrifuge tube was cut, and each phase was transferred to a scintillation vial. The phase containing the dissolved cells was neutralized with 50 μl of 2 N HCl, mixed with scintillation cocktail, and its radioactivity was measured in a liquid scintillation counter (LS6000SE; Beckman Coulter). The time course for the uptake of [^{3}H]pravastatin into hepatocytes was expressed as the uptake volume (microliters per 10^6 viable cells) of the radioactivity taken up into the cells (disintegrations per minute per 10^6 cells) divided by the concentration of radioactivity in the incubation buffer (disintegrations per minute per microliter). The initial uptake velocity of [^{3}H]pravastatin was calculated from the slopes of the uptake volume versus time plots

obtained at 0.5 and 2 min and expressed as the uptake clearance (microliters per minute per 10^6 cells).

Metabolism Study Using the Liver S9 Fraction

It has been reported that pravastatin is metabolized by sulfotransferase in male rats (Kitazawa et al., 1993). Therefore, we used the liver S9 fraction as the enzyme source. The liver S9 fraction was prepared from four rats using standard procedures and stored at −80°C until use. The protein concentration was determined by the Lowry method, using bovine serum albumin as the standard. Pravastatin was incubated with a reaction mixture consisting of rat liver S9 fraction (final concentration, 8 mg/ml), NADPH-generating system (0.8 mM $NADP^+$, 8 mM glucose 6-phosphate, 1 U/ml glucose-6-phosphate dehydrogenase, and 3 mM $MgCl_2$), and 3′-phosphoadenosine 5′-phosphosulfate (final concentrations, 0.5 and 5 mM for low and high pravastatin concentrations, respectively) in the presence of 100 mM phosphate buffer, pH 7.4. After preincubation at 37°C for 10 min, pravastatin (final concentration, 0.1–500 μM) was added to initiate the enzyme reaction. At the designated time, the reactions were terminated by mixing them with equal volumes of methanol containing R-122798, an analytical internal standard, followed by centrifugation at 15,000*g* for 10 min at 4°C. The supernatant was subjected to liquid chromatography/mass spectrometry (LC/MS) analysis. In studies with the human liver S9 fraction, the concentrations of pravastatin and 3′-phosphoadenosine 5′-phosphosulfate were 5 μM and 1 mM, respectively; other incubation conditions were the same as in the rat studies.

LC/MS Analysis

Liver, kidney, brain, lung, and skeletal muscle were added to 3 to 5 volumes of physiological saline (w/v) and homogenized. Tissue homogenates and plasma, bile, and urine samples were deproteinated with 2 volumes of methanol containing the internal standard (1 μg/ml R-122798) and centrifuged at 15,000*g* for 10 min at 4°C. High-concentration samples were diluted appropriately with blank matrix before deproteination. The supernatant was subjected to LC/MS analysis. The appropriate standard curves were prepared in the equivalent blank matrix and used for each analysis.

The LC/MS consisted of an Alliance HT 2695 separation module with an autosampler (Waters, Milford, MA) and a Micromass ZQ mass spectrometer with an electron ion spray interface (Waters). The optimum operating conditions used were as follows: electrospray probe (capillary) voltage, 3.2 kV; sample cone voltage, 20 V; and source temperature, 100°C. The spectrometer was operated at a drying desolvation gas flow rate of 350 l/h. The mass spectrometer was operated in the selected ion monitoring mode using the respective MH− ions, *m/z* 423.3 for pravastatin and *m/z* 409.3 for the internal standard. The mobile phase used for high-performance liquid chromatography was acetonitrile/ammonium acetate buffer (10 mM), pH 4 = 7:3 (v/v), and the flow rate was 0.3 ml/min. Chromatographic separation was achieved on a C18 column (Inertsil ODS-3 column, 50 × 2.1 mm; particle size, 3 μm) (GL Sciences, Tokyo, Japan).

Data Analysis of Metabolic Clearance in Liver S9

The metabolic velocity was calculated from the slope of the natural log (concentration)-time plot. Because the Eadie-Hofstee plot showed curvature, the kinetic parameters were obtained using eq. 1:

$$v = \frac{V_{max1} \times S}{K_{m1} + S} + \frac{V_{max2} \times S}{K_{m2} + S} \quad (1)$$

where v is the initial velocity (picomoles per minute per milligram of protein), S is the substrate concentration (micromolar), V_{max1} and V_{max2} are the maximum velocities (picomoles per minute per milligram of protein), and K_{m1} and K_{m2} are the Michaelis constants (micromolar). Fitting was performed with the nonlinear least-squares method using the MULTI program (Yamaoka et al., 1981). The input data were weighted as the reciprocals of the observed values, and the Damping Gauss-Newton algorithm was used for fitting.

Model Development

The PBPK model was constructed to describe the pharmacokinetics of pravastatin in rats and humans (Fig. 1). The key features of this model are as follows. 1) Active uptake (PS_{inf}) and passive diffusion clearances (PS_{dif}) on the sinusoidal membrane, and biliary clearance (PS_{bile}) on the canalicular membrane in the liver are incorporated. 2) The liver compartment consists of five units of extracellular and subcellular compartments, connected by blood flow in tandem, to fit the hepatic disposition to the "dispersion" model. Because the hepatic elimination of pravastatin in rats is blood flow limited, the dispersion model is the appropriate model for the hepatic elimination of such high-clearance drugs (Roberts and Rowland, 1986; Iwatsubo et al., 1997; Naritomi et al., 2001). The number of liver compartments was determined by comparing the hepatic availability ($F_{h,n}$) and F_h predicted using the dispersion model. $F_{h,n}$ is the product of the availability in the liver compartments (eq. 2).

$$F_{h,n} = (Q/(Q + f_B(CL_{int,all}/n)))^n \quad (2)$$

where n represents the number of compartments. The integer number n, which gave the $F_{h,n}$ value closest to that in the dispersion model, was selected. 3) The brain and muscle, target tissues for the adverse effects of statins, were included. 4) Although urinary excretion is a minor elimination pathway in male rats, the kidney was included because the kidney/blood concentration ratio for pravastatin is high in male rats, probably because of the efficient uptake and/or reabsorption of pravastatin. The renal clearance of pravastatin in male rats was lower than the glomerular filtration rate corrected by the blood unbound fraction. In contrast, renal clearance must be taken into consideration in humans. Because this study focused on hepatobiliary transport, renal elimination occurs from the systemic compartment. 5) The rapid equilibrium distribution of pravastatin between the blood and tissues other than the liver was assumed. 6) The initial distribution volume, estimated by fitting the plasma concentration time profiles of pravastatin in rats after the

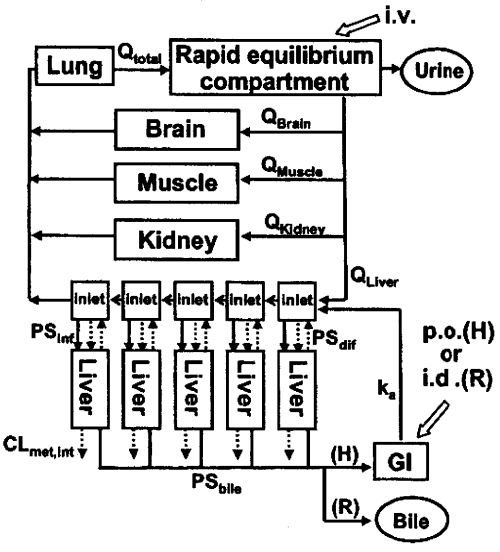

Fig. 1. Schematic diagram of the PBPK model predicting the concentration-time profiles of pravastatin. The liver compartment was divided into five compartments to mimic the dispersion model. Indicated are the blood flow (Q), the active hepatic uptake clearance (PS_{inf}), the passive diffusion clearance (PS_{dif}), the biliary clearance (PS_{bile}), and the metabolic clearance ($CL_{met,int}$), human (H), and rat (R). The enterohepatic circulation was incorporated in the case of humans.

intravenous administration of 0.2 and 1 mg/kg to a two-compartment model, was used as the volume of the rapid equilibrium compartment including the blood compartment, and it was assumed that there is no interspecies difference in the initial distribution volume. The differential equations are shown in Appendix I, and all simulations were performed with SAAM II (SAAM Institute, Seattle, WA).

Estimation of Kinetic Parameters Used in the Simulation

In Vitro Parameters (Rats and Humans). The in vitro active uptake ($PS_{inf,vitro}$) and passive diffusion clearances ($PS_{dif,vitro}$) of pravastatin on the sinusoidal membrane were determined from the uptake studies using isolated hepatocytes. The parameters for rats were taken from previous reports (Yamazaki et al., 1993; Ishigami et al., 1995), and those for humans were determined in the present study. $PS_{inf,vitro}$ and $PS_{dif,vitro}$ were regarded as the saturable and nonsaturable components, respectively, in the uptake clearance into hepatocytes. A physiological scaling factor of 1.2×10^8 cells/g liver was used for scaling up to the organ level (Iwatsubo et al., 1997). The in vitro biliary clearance ($PS_{bile,vitro}$) of pravastatin was calculated from the ATP-dependent uptake clearance into the CMVs using eq. 3 (Niinuma et al., 1999):

$$PS_{bile,vitro} = (V_{initial} \times R)/(E \times IO) \quad (3)$$

where $V_{initial}$ represents the velocity of the initial ATP-dependent uptake by CMVs corrected by medium concentration (6.08 μl/min/mg protein for rats and 1.90 μl/min/mg protein for humans), R represents the recovery of liver homogenate protein (174 mg homogenate protein/g liver for rats and 133 mg homogenate protein/g liver for humans), E represents the enrichment of the CMV fraction (70.4 for rats and 61.8 for humans), and IO represents the population of inside-out CMVs (0.347 for rats and 0.555 for humans).

In Vivo Parameters (Rats). The in vivo intrinsic biliary clearance ($PS_{bile,vivo}$) at the canalicular membrane was calculated by dividing the biliary excretion rate by the hepatic unbound concentration at steady state (Yamazaki et al., 1996b, 1997). Systemic elimination other than biliary excretion was regarded as the hepatic metabolism because renal elimination in male rats is negligible. Thus, in vivo intrinsic metabolic clearance ($CL_{met,int,vivo}$) was obtained with eq. 4:

$$CL_{met,int,vivo} = PS_{bile,vivo} \times \frac{100 - (\%\text{ of excretion into bile at 0.2mg/kg})}{(\%\text{ of excretion into bile at 0.2mg/kg})} \quad (4)$$

The in vivo passive diffusion clearance on the sinusoidal membrane was assumed to be the same as $PS_{dif,vitro}$. The in vivo active uptake clearance ($PS_{inf,vivo}$) was estimated using eq. 5:

$$PS_{inf,vivo} = CL_{int,all} \times \frac{PS_{dif,vivo} + PS_{bile,vivo} + CL_{met,int,vivo}}{PS_{bile,vivo} + CL_{met,int,vivo}} - PS_{dif,vivo} \quad (5)$$

where $CL_{int,all}$ represents the overall hepatic intrinsic clearance estimated from the hepatic availability using the dispersion model, with a dispersion number of 0.17, which was obtained by dividing the bioavailability by the fraction absorbed (Komai et al., 1992), assuming negligible metabolism in the small intestine. The average of the tissue/blood concentration ratios at 30, 60, and 90 min after the intravenous administration at 10 mg/kg pravastatin were used as the tissue/blood partition coefficient (K_p), assuming a pseudo-steady state (Table 2). Actually, the tissue/blood concentration ratios at 30, 60, and 90 min were similar (muscle, 0.28, 0.21, and 0.18; brain, 0.045, 0.029 and 0.034; kidney, 13, 14, and 15; lung, 0.76, 0.67, and 0.77 at 30, 60, and 90 min, respectively). The absorption rate constants were estimated by noncompartment analysis using the plasma concentration data.

Results

In Vivo Pharmacokinetics of Pravastatin in Rats. Figure 2 shows time profiles of the plasma concentration of pravastatin after its intravenous (0.2 mg/kg) and intraduodenal (20 mg/kg) administration and the cumulative amount of pravastatin excreted into the bile. The total blood clearance ($CL_{tot,B}$) was similar to the hepatic blood flow rate. The bioavailability of pravastatin after intraduodenal administration was calculated to be 0.0087 by comparing the AUC for pravastatin after intravenous and intraduodenal administration. Forty-six percent of the dose was recovered in the bile as the parent compound after intravenous administration, whereas the amount excreted into the urine was less than 4% of the dose. Even after intraduodenal administration, 33% was recovered in the bile.

The nonlinearity of the disposition of pravastatin was examined. The plasma concentrations and cumulative amounts excreted into the bile after its intravenous administration were determined at doses ranging from 0.2 to 200 mg/kg (Fig. 3). $CL_{tot,B}$ was independent of the dose up to 50 mg/kg but decreased to 27 ml/min/kg at 200 mg/kg pravastatin. The cumulative biliary excretion increased slightly from 46 to 60% at doses above 0.2 mg/kg and was significantly delayed at 200 mg/kg.

Hepatic Metabolism of Pravastatin in Rats. The metabolism of pravastatin in the liver was examined using S9 fractions prepared from rat liver. It exhibited biphasic kinetics with high-affinity (K_{m1}, 0.846 ± 0.403 μM; V_{max1}, 4.47 ± 1.92 pmol/mg/min) and low-affinity (K_{m2}, 80.3 ± 12.6 μM; V_{max2}, 240 ± 16.2 pmol/mg/min) components (mean ± S.D.). The sum of the in vitro metabolic clearance for the high- and low-affinity components, corrected with the physiological scaling factor of 96.1 mg protein/g liver, was used as the in

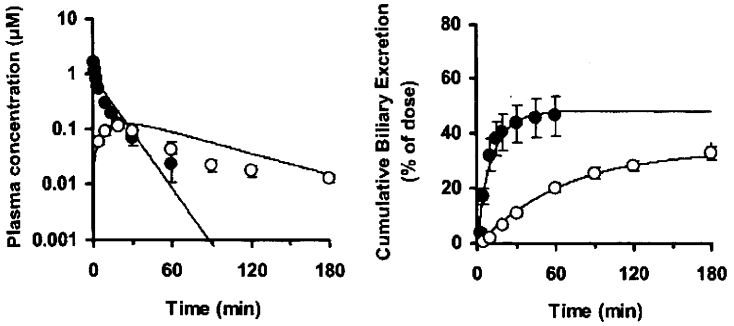

Fig. 2. Simulated and observed plasma concentrations and biliary excretion rates for pravastatin in rats after intravenous (●, 0.2 mg/kg) or intraduodenal (○, 20 mg/kg) administration. The symbols and solid lines represent experimentally observed and simulated values, respectively. Each point represents the mean ± S.E. (n = 3).

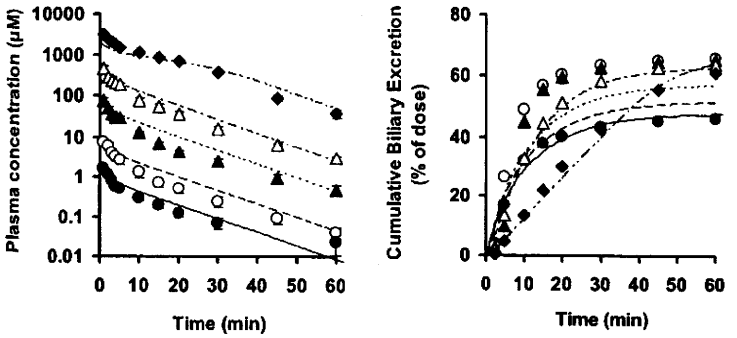

Fig. 3. Simulated and observed plasma concentrations and biliary excretion rates for pravastatin in rats after the intravenous administration of various doses. The symbols and lines represent experimentally observed and simulated values, respectively. Each point represents the mean ± S.E. (n = 3). ——— ●, 0.2 mg/kg; - - - - ○, 1 mg/kg; · · · · · · · · · , 10 mg/kg; —· — · — △, 50 mg/kg; —· · —· ♦, 200 mg/kg.

vitro metabolic clearance ($CL_{met,int,vitro}$), which was 0.793 ml/min/g liver (Table 1).

Simulation of Concentration-Time Profiles of Pravastatin in Rats. All parameters used in the simulation are summarized in Tables 1 and 2. The initial distribution volume was estimated to be 0.393 l/kg from the plasma concentration profile after the intravenous administration of 0.2 mg/kg pravastatin, which was used as the volume of the rapid equilibrium compartment in the model. Figures 2 and 3 show the simulated plasma concentrations and biliary excretion time profiles for pravastatin, together with the observed data after its intravenous and intraduodenal administration. To reproduce the in vivo pharmacokinetic profiles using in vitro parameters, SFs were necessary. For the in vitro-in vivo extrapolation of the transporter-mediated clearances, the ratio of the in vivo/in vitro intrinsic clearances of each process in rats was given as the SF (Table 1). Furthermore, using the K_m values, the simulated plasma concentration and biliary excretion time profiles gave similar values to the observed data, even under nonlinear conditions. This model reproduced the time profiles for pravastatin in the liver and other peripheral tissues after its intravenous administration (Figs. 4 and 5). In particular, the nonlinearity of the liver concentration-time profiles could also be simulated (Fig. 4). Although the model reasonably describes the experimental data, the simulated lines showed some deviation from the observed data at the terminal phase in Figs. 2 (left) and 5. This may be caused by the lack of a compartment corresponding to the organ, which is associated with the terminal phase of systemic pravastatin. Moreover, the simulation results of biliary excretion of pravastatin administered at 1 and 10 mg/kg showed some deviation from the observed data (Fig. 3, right). Because hepatic metabolism is saturated at these doses, this may be attributed to the deviation of the K_m value for metabolism.

Prediction of Pharmacokinetics in Humans. The uptake clearance determined using eight lots of human cryopreserved hepatocytes was 4.5 ± 2.9 μl/min/10^6 cells at 1 μM pravastatin and 0.77 ± 0.63 μl/min/10^6 cells at 100 μM pravastatin (mean ± S.D.). Using the physiological scaling factor of 1.2×10^8 cells/g liver, $PS_{inf,vitro,human}$ and $PS_{dif,vitro,human}$ were calculated to be 0.448 and 0.0924 ml/min/g liver, respectively (Table 1). Unlike the rat liver S9 fraction, no metabolism of pravastatin was observed up to 180 min in the human liver S9 fractions purchased from three different vendors. Thus, the hepatic metabolism of pravastatin might be negligible in the human liver. The in vivo kinetic parameters for pravastatin in humans were predicted by multiplying the corresponding in vitro parameters obtained using human materials by the SF obtained from rat studies. For PS_{bile}, the saturable (ATP-dependent) biliary clearance in humans was predicted as described above (eq. 3), and the nonsaturable component of the biliary clearance in humans was assumed to be the same as that in rats. Thus, the predicted $PS_{bile,\ vivo,\ human}$ was 0.388 ml/min/g

TABLE 1

Kinetic parameters for hepatic intrinsic clearance

Active hepatic uptake and passive diffusion clearances on the sinusoidal membrane, biliary clearance on the canalicular membrane, and metabolic clearance were estimated by both in vitro and in vivo experiments. The details of these estimations are described in the text. Values within parentheses indicate the K_m value (micromolar) for each clearance.

	Rat		Scaling Factor	Human	
	In Vitro	In Vivo		In Vitro	In Vivo*
	ml/min/g liver			*ml/min/g liver*	
PS_{inf}	2.47[a,b] (32.8)	9.06[g]	3.7	0.448	1.66
PS_{dif}	0.192[a,b]	0.192[e]	1[e]	0.0924	0.0924
PS_{bile}					
ATP-dependent	0.0433[c]	0.906[d] (92.3)	21	0.00737[c]	0.154
Nonsaturable		0.234[d]			0.234[f]
$CL_{met,int}$	0.793 (0.846, 80.3)	1.33[h]	1.7	0	0

* Predicted by multiplying the in vitro parameter by the SF.
[a] Yamazaki et al. (1993).
[b] Ishigami et al. (1995).
[c] Calculated using eq. 3 (Niinuma et al. (1999)).
[d] Yamazaki et al. (1997).
[e] Assumed that the SF for PS_{dif} is 1.
[f] Assumed negligible interspecies difference between rat and human.
[g] Calculated using eq. 5.
[h] Calculated using eq. 4.

TABLE 2
Physiological and kinetic parameters for modeling in rats and humans

	Rat	Human
Physiological Parameters		
Weight (g/kg)[a]		
Liver	41.2	24.1
Extracellular space in liver	11.5	6.7
Brain	6.8	5.3
Lung	4.0	16.7
Muscle	488	429
Kidney	9.2	4.43
Blood flow rate[a] (ml/min/kg)		
Liver	55.2	20.7
Brain	5.3	10.0
Lung	172	74.9
Muscle	30.0	10.7
Kidney	36.9	15.7
Kinetic parameters		
Plasma unbound fraction[b]	0.64	0.47
Liver unbound fraction	0.51[c]	0.51[d]
Blood/plasma ratio[c]	0.59	0.56
Fraction absorbed	0.62[f]	0.47[g]
Renal clearance (ml/min/kg)	1.5[h]	11.3[i]
Absorption rate constant (min^{-1})[j]	0.0088	0.0078
Tissue/blood concentration ratio		
Brain	0.036	0.033[k]
Lung	0.74	0.67[k]
Muscle	0.22	0.20[k]
Kidney	14	13[k]

[a] The volume and blood flow rate in each tissue were taken from Davies and Morris (1993) and Kawai et al. (1994). The tissue volume was converted to tissue weight based on the assumption that the tissue gravity is 1 g/ml.
[b] Yamazaki et al. (1996c) and manufacturer's interview form.
[c] Yamazaki et al. (1996b).
[d] Assumed negligible interspecies difference between rat and human.
[e] Yamazaki et al. (1996c) and Lennernäs and Fager (1997).
[f] Komai et al. (1992).
[g] Estimated from the bioavailability (0.18) and hepatic availability (0.38) (Singhvi et al., 1990).
[h] Obtained from the urinary excretion data for intravenous administration of 10 mg/kg.
[i] Singhvi et al. (1990).
[j] Estimated by noncompartment analysis.
[k] Estimated by $K_p = f_B/f_T$.

liver. Assuming that the distribution of pravastatin to the tissues, except the liver, occurs by passive diffusion, the tissue/blood partition coefficient (K_p) was calculated by the following equation: $K_p = f_B/f_T$, where f_B and f_T represent the blood unbound fraction (=plasma unbound fraction/blood-to-plasma concentration ratio) and the unbound fraction in the tissues, respectively. It was assumed that there is no species difference in f_T between rats and humans based on the previous report by Sawada et al. (1985). The estimated or reported physiological, anatomical, and kinetic parameters for humans used in the simulation are shown in Tables 1 and 2. Using these parameters, the plasma concentration-time profiles for pravastatin in humans after intravenous or oral administration were predicted. A lag time of 17 min was taken into consideration in the simulation of oral administration. The predicted concentration-time profiles were similar to the observed data (Fig. 6).

Effect of Transporter Activity on Systemic and Target Exposure. Sensitivity analyses were performed to understand the effects of the changes in transporter activities on the time profiles for the plasma and liver (a target organ) concentrations of pravastatin in humans. The plasma and liver concentrations after the oral administration (40 mg) of pravastatin were simulated using the PBPK model constructed in this study, with varying hepatic transport activities over a range of 0.33 to 3.0 times the initial value. The simulated concentration-time profiles and the changes in the AUC are shown in Fig. 7 and Table 3, respectively. Changes in the active hepatic uptake ability affected the plasma concentration profiles dramatically but did not greatly affect the liver concentration profiles. On the contrary, changes in the ability of canalicular efflux altered the liver concentration of pravastatin markedly but had a small effect on the plasma concentration. Changes in the passive diffusion clearance hardly affect the plasma and the liver concentration profiles.

Discussion

It is now well recognized that drug transporters play important roles in the processes of absorption, distribution, and excretion (Giacomini and Sugiyama, 2005; Shitara et al., 2006a). The purpose of this study was to construct a PBPK model to evaluate the concentration-time profiles for drugs in the plasma and peripheral organs in humans using physiological parameters, SFs, and drug-related parameters (unbound fraction and metabolic and membrane transport clearances extrapolated from in vitro experiments). The principle of the prediction was as follows. First, SFs were obtained by comparing in vitro and in vivo parameters in rats. Then, the in vitro human parameters were extrapolated in vivo using the SFs obtained in rats (Naritomi et al., 2001). Pravastatin was selected as the model compound because many studies have investigated the mechanisms involved in the drug disposition in rodents, and clinical data after intravenous and oral administration are available.

Consistent with a previous report (Yamazaki et al., 1996a), the hepatic elimination of pravastatin is blood flow limited. Considering that the maximum amount of intact pravastatin excreted into the bile was 50%, it is likely that pravastatin undergoes hepatic metabolism in rats because pravastatin is excreted negligibly in the urine. Incubating pravastatin with the rat liver S9 fractions caused a reduction in intact pravastatin with time and consisted of two different mechanisms with high- and low-affinity sites. The kinetic parameters related to hepatic clearance (PS_{inf}, PS_{dif}, PS_{bile}, and $CL_{met,int}$) were estimated from various in vivo experiments and were incorporated into the PBPK model. As a result, plasma concentration and biliary excretion-time profiles for pravastatin were successfully reproduced (Figs. 2–5). Moreover, nonlinear pharmacokinetics were also reproduced using the K_m values for hepatic uptake, biliary excretion, and metabolic clearances (Fig. 3). The liver concentrations of pravastatin were similar to the observed data,

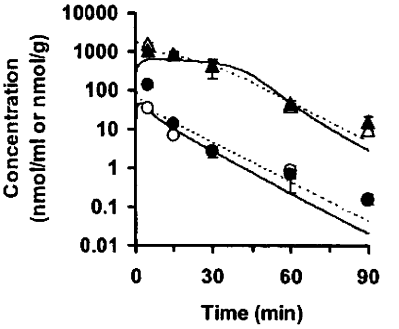

Fig. 4. Simulated and observed liver concentration profiles for pravastatin in rats after intravenous administration. Dashed and solid lines, simulated plasma and liver concentrations, respectively. Open and closed symbols, experimentally observed plasma and liver concentrations, respectively (circles, 10 mg/kg; triangles, 200 mg/kg). Each point represents the mean ± S.E. (n = 3).